Alma Mater Studiorum · Università di Bologna

SCUOLA DI SCIENZE

Corso di Laurea Magistrale in Fisica del Sistema Terra

Long-period oscillations in GPS Up time series. Study over the European/Mediterranean area

Relatore:

Prof.ssa Susanna Zerbini

Presentata da:

Anna Fantoni

Correlatori:

Prof.ssa Damiana Lazzaro
Dr.ssa Letizia Elia

Sessione III
Anno Accademico 2020-2021

Abstract

English version

The surface of the Earth is subjected to vertical deformations caused by geophysical and geological processes which can be monitored by Global Positioning System (GPS) observations. The purpose of this work is to investigate GPS height time series to identify interannual signals affecting the Earth's surface over the European and Mediterranean area, during the period 2001-2019. Thirty-six homogeneously distributed GPS stations were selected from the online dataset made available by the Nevada Geodetic Laboratory (NGL) on the basis of the length and quality of the data series.

The Principal Component Analysis (PCA) is the technique applied to extract the main patterns of the space and time variability of the GPS Up coordinate. The first three principal components of the GPS Up coordinate time series were studied by means of a frequency analysis using a periodogram and the real-valued Morlet wavelet. The periodogram is used to identify the dominant frequencies and the spectral density of the investigated signals; the second one is applied to identify the signals in the time domain and the relevant periodicities. The wavelet analysis is a technique by a better resolution than the periodogram and it allows investigating lower frequencies.

This study has identified, over European and Mediterranean area, the presence of interannual non-linear signals with a period of 2-to-4 years, possibly related to atmospheric and hydrological loading displacements and to climate phenomena, such as El Niño Southern Oscillation (ENSO). A clear signal with a period of about six years is present in the vertical component of the GPS time series, likely explainable by the gravitational coupling between the Earth's mantle and the inner core. The results are in good agreement with recent studies published in the relevant literature. Moreover, signals with a period in the order of 8-9 years, might be explained by mantle-inner core gravity coupling and the cycle of the lunar perigee, and a signal of 18.6 years, likely associated to lunar nodal cycle,

were identified through the wavelet spectrum. However, these last two signals need further confirmation because the present length of the GPS time series is still too short when compared to the periods involved.

La superficie della Terra è soggetta a deformazioni verticali causate da processi geofisici e geologici che possono essere monitorati con osservazioni GPS (Global Positioning System). L'obiettivo di questa tesi è quello di investigare le serie temporali delle quote GPS per identificare segnali interannuali che influenzano la superficie terrestre in Europa e nel Mediterraneo, nel periodo temporale 2011-2019. Trentasei stazioni GPS, omogeneamente distribuite sull'area di interesse, sono state selezionate dagli archivi del Nevada Geodetic Laboratory (NGL) sulla base della lunghezza e della qualità delle serie di dati.

L'analisi delle componenti principali (PCA) è la tecnica che è stata adottata per estrarre i principali pattern di variabilità spaziale e temporale della coordinata verticale del GPS. Le prime tre componenti principali delle serie temporali della coordinata Up del GPS sono state studiate con l'utilizzo del periodogramma e delle real-valued Morlet wavelet. Il periodogramma si usa per identificare le frequenze dominanti e la densità spettrale dei segnali investigati; il secondo si adotta per identificare i segnali nel dominio dei tempi e le periodicità rilevanti. L'analisi wavelet è una tecnica caratterizzata da una migliore risoluzione rispetto al periodogramma e permette di investigare frequenze minori.

Questo studio ha identificato, sull'area europea e mediterranea, la presenza di segnali interannuali non lineari con un periodo tra 2 a 4 anni, potenzialmente legati al caricamento atmosferico e idrologico, come El Niño Southern Oscillation (ENSO). Un chiaro segnale con un periodo di circa sei anni è presente nella componente verticale delle serie temporali del GPS, probabilmente spiegabile dall'accoppiamento gravitazionale tra il mantello e il nucleo interno della Terra. I risultati sono in linea con gli studi recentemente pubblicati in letteratura. Inoltre, segnali con un periodo nell'ordine di 8-9 anni, che potrebbero essere spiegati dall'accoppiamento gravitazionale tra il mantello e il nucleo interno e dal ciclo del perigeo lunare, e un segnale di 18.6 anni, probabilmente legato al ciclo del nodo lunare, sono stati identificati per mezzo dello spettro wavelet. Tuttavia, questi ultimi due segnali necessitano di ulteriori conferme dal momento che la lunghezza delle odierne serie temporali del GPS è ancora troppo breve quando confrontata con i periodi coinvolti.

Contents

List of Figures

List of Tables

Chapter 1

Introduction

The Earth surface is subjected to both horizontal and vertical deformations. They are due to a number of geophysical and geological processes acting at different spatial and temporal scales. Time scales range from seconds, in the case of seismic events, to millions of years, for plate tectonics. Spatial scales range from local to global, examples are subsidence for the local case, and the glacial isostatic adjustment (GIA) for the global dimension.

The Global Positioning System (GPS), a satellite-based radio navigation system, provides accurate data to investigate surface deformation. Today GPS is also referred to as GNSS (Global Navigation Satellite System) which encompasses similar positioning systems such as GLONASS and Galileo.

Nowadays, time series of GPS coordinates of thousands of stations, globally distributed, are available. They are provided by Services of the International Association of Geodesy (IAG) or by other Institutions such as the Nevada Geodetic Laboratory (NGL `http://geodesy.unr.edu`).

In this thesis, GPS height time series of stations located over the European and Mediterranean area were analyzed, with the aim to identify long-period oscillations whose origin can likely be explained. GPS height time series are characterized by both short- and long-period variations which need to be identified and removed before estimating linear trends. Well-known short-period oscillations are those occurring at seasonal scale (annual) (Elia et al., 2021). In general, they are the most prominent short-period feature characterizing the GPS height time series. The annual signal is explained by the superposition of loadings on the Earth's crust caused by the atmosphere, terrestrial water storage and tidal and non-tidal oceanic components.

Interannual variations of GPS heights were studied in relation to changing climate and variability of environmental parameters (Tiwari et al., 2014; Elia et

al., 2021). Interdecadal fluctuations, observed in the GPS height time series, were associated by Ding et al., 2018, and by Pan et al., 2019, to variations of the length of day (LOD), likely explainable by processes of core-mantle coupling according to Ding, 2019, and Ding et al., 2021. Height variability is also characterized by long-period signals of tectonic nature.

Long-period signatures are recognized in time series of several parameters of geodetic/geophysical nature. Two interesting examples are the periodic intradecadal oscillations of about six (SYO) and about eight years (EYO). The SYO had been detected by Vondrak in 1997 by analysing the difference between the rotational time UT1 and atomic time scale AT over the period 1958-1969. It was confirmed by Liao and Greiner-Mai (1999) who studied the atmospheric angular momentum (AAM) monthly series from 1968 to 1997.5 provided by the NCEP (National Centers for Environmental Prediction) and the LOD series. They found a $\sim$ 5.6 years oscillation and a peak-to-peak amplitude of about 0.3 ms in the residuals suggesting that the ΔLOD were excited by other geophysical processes rather than the atmospheric excitation, which resulted too small on the decadal time scale. Mound and Buffett (2003, 2006) studied the AAM and LOD series and came to the conclusion that this oscillation can be explained by the gravitational coupling between the Earth's mantle and the inner core, and estimated that the period of the SYO was approximately 5.8 $\pm$ 0.8 year. They proposed a theoretical model of the core-mantle system that allows to calculate the natural period of interannual oscillations in the axial rotation of the core and mantle. During the recent years several other investigations were developed, regarding the SYO, by making use of GPS time series (Ding et al., 2018; Pan et al., 2019), which are accurate and long enough to study this type of phenomena.

The EYO was also detected in the ΔLOD, i.e. Ding (2019), by using two datasets, the first one is a yearly LOD time series over the period 1962-2016 and the second one was obtained from the analysis of the Earth Orientation Parameters EOPC04 (`ftp://hpiers.obspm.fr/eop-pc/eop`) dataset, identified an oscillation with period of about 8.5 years. According to Duan and Huang (2020), this signal is likely explained by fast equatorial waves, named QG Alfvén waves, propagating at Earth's core surface and it may have correlation with geomagnetic jerks (Ding et al., 2021).

Ding (2019) detected other interdecadal signals with periods of about 11, 13, 18.6, 22.3 years and more. While the 18.6 years signal is generated by a well

known process due to the Lunar nodal cycle, the physical processes causing all the other signals are still not clearly demonstrated (Ding et al., 2021).

The thesis examines Europe and the Mediterranean because in this continental area a dense network of permanent GPS stations, with rather long time series, is available. The stations were selected considering the data quality, the length of the time series and on the basis of their location, in order to obtain a spatial distribution as homogeneous as possible. The GPS height time series analysed were acquired from an online data set made available by the NGL (`http://geodesy.unr.edu/PlugNPlayPortal.php`).

From now on, the height series will be referred to as Up time series (see chapter 2). The Up series of the selected stations underwent a pre-processing phase during which outliers, offsets, linear trends and the seasonal signal were detected and removed. Spline functions were applied to the residual series thus obtained in order to interpolate the missing data. The Principal Component Analysis (PCA) method (see chapter 3) was used to study the spatial and temporal variability of the Up component over the area of interest. The periodogram was used to identify the signal frequency and its magnitude. Therefore, the real-valued Morlet wavelet transforms (see chapter 4.2) were applied to the time series to identify the long-period signals and to study their evolution in the time domain and their periodicity.

The analysis of the GPS Up time series has allowed to clearly identify a signal with a period of about 5.72 years and, in addition, shorter-period oscillations (2-to-4 years), likely related to hydrological loading displacements (Pan et al., 2019). Identifying vertical surface deformations is important in the light of understanding the dynamic processes governing these oscillations and eventually contributing to the realisation of accurate physical models. Removing known and large signals from the GPS Up time series leads to the possibility of identifying and studying weaker signatures.

1.1 Global Positioning System

The Global Positioning System is a satellite-based radio navigation system providing precise three-dimensional position, navigation, and time information to suitably equipped users Seeber, 2008. It was originally developed in the 70s by the U.S. Department of Defense, for military purposes. In May 2000, it was extended to civil and commercial users, it is used to solve geodetic duties since 1983.

The GPS constellation consists of 24 satellites placed in orbits at about 20.200 km altitude above the Earth's surface. The arrangement is intended to allow the view of, at least, four satellites simultaneously. Three satellites enable the determination of the geometrical position. The fourth one is necessary because GPS is a one-way ranging technique[1]; therefore, the receiver and the satellite clocks are not synchronized. GPS is a navigation system, based on the measurement of the so-called pseudoranges between the user and the four satellites. The synchronization error is the reason for the term pseudorange. By knowing the coordinates of the satellite in a suitable reference frame, the coordinates of the user antenna can be determined.

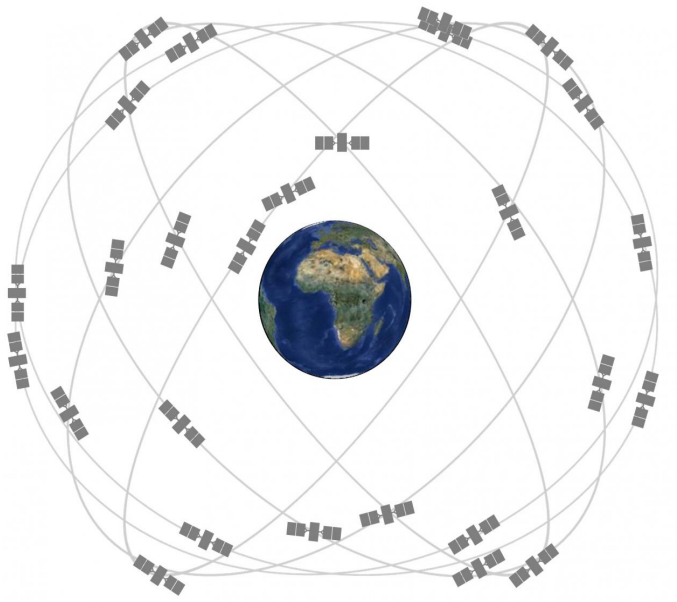

Figure 1.1: Global Position System constellation of 24 satellites.

Each satellite transmits three signals modulated onto two carrier frequencies

[1]In the one-way mode it is assumed that either the clocks in the satellite and in the receiver are synchronized with each other or that a remaining synchronization error can be determined through the observation technique (Seeber, 2003).

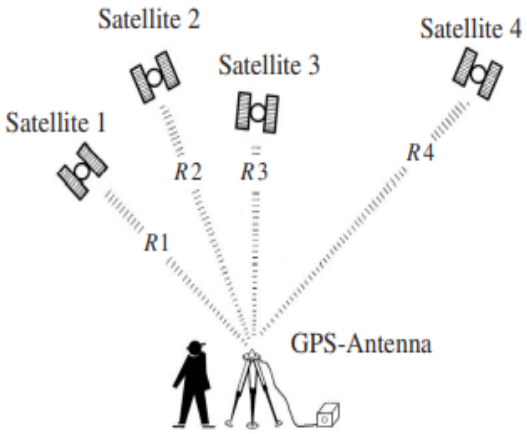

Figure 1.2: Principle of positioning with GPS (from Seeber, 2003).

L1 and L2; these are the navigation signals (codes) and the navigation and system data (message). The codes are modulated on the carrier frequencies as so-called pseudo random noise (PRN) sequences. The L1 signal contains both P-code and C/A-code[2], the L2 signal contains just the P-code. The third signal is the broadcast message.

The GPS signal is affected by a few perturbations due to the fact that it travels through the atmosphere. The ionosphere[3] and the dry and wet components of the troposphere[4], which cause a delay in the signal propagation. The ionospheric delay depends on the frequency, the geographic location and time; therefore, the error[5] can be adjusted by using a dual-frequency code geometry-free combination. The tropospheric delay is related to the signal path through the neutral atmosphere, thus it can be modelled as a function of the satellite elevation angle. The dry component error can be corrected by using a simple model, whereas the delay caused by the wet component is more unpredictable and an appropriate correction can only be achieved by using mapping functions such as the Vienna (Böhm and Schuh, 2003) and by determining atmospheric parameters when estimating the position solutions.

[2]The P-code (precision or protected) and the C/A-code (clear/acquisition) are the modulation codes, expressed as a series of -1/+1.

[3]the ionosphere is the upper part of the atmosphere between around 70 and 1000 km.

[4]The troposphere is the lower part of the atmosphere extends from the surface to about 10 to 15 km. The dry component is due to the presence of dry gases, such as nitrogen, oxygen, argon and others; it affects the local temperature and the atmospheric pressure. The wet component is caused by the water vapor and condensed water, thus it varies according to the weather conditions.

[5]The resulting error for GPS frequencies is in a range between less than 1 m to more than 100 m.

1.1.1 GPS coordinate system

The coordinates used for the study are the Earth-Centered Earth-Fixed (ECEF) and the East, North and Up (ENU), defined with respect to the reference ellipsoid[6].

The ECEF coordinate system is also called "conventional terrestrial" coordinate system; its origin is in the center of the Earth, the z axis is directed toward the North Pole, the x axis toward the prime Greenwich meridian and the y axis completes the triad of coordinates. This system co-rotates with the Earth, therefore the coordinates of stationary points on the surface of the Earth do not vary (figure 1.3).

The local ENU coordinates are formed from a plane tangent to the surface of the Earth fixed to a specific location, where the East direction follows the circle of latitude, the North direction follows the local meridian and the Up is orthogonal to east and north axis, outward with respect to the surface of the Earth (1.3).

This work analyses the time series of the Up component. They describe the vertical displacements of the stations which are part of the study.

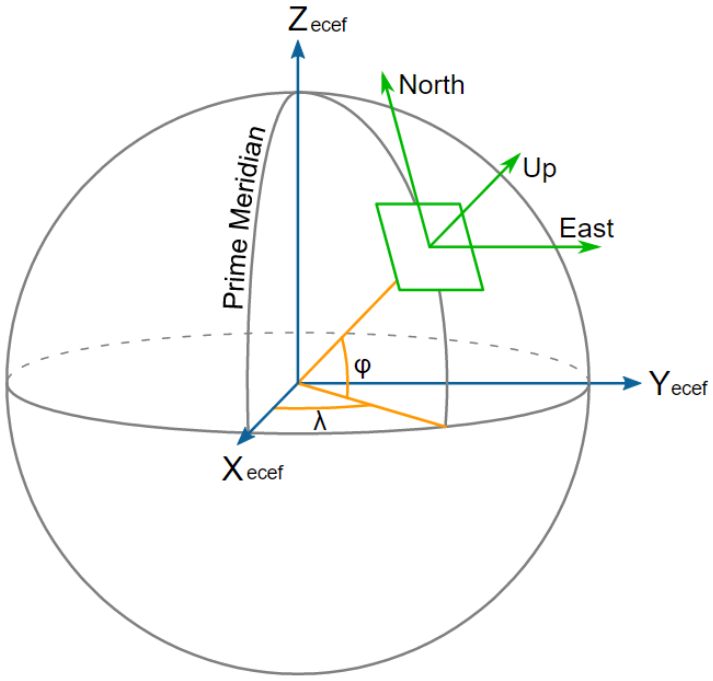

Figure 1.3: ENU and ECEF coordinate systems

[6]mathematical surface which approximate the geoid, which is the physical representation of the Earth

Chapter 2

Data pre-processing

The focus of this study is to analyse the Up time series of stations located in the European and Mediterranean area with the objective to identify long-period signals which may be originated by different physical processes. To this aim, daily GPS Up time series, which describe the vertical surface displacements, were used.

Thirty-six stations were selected on the basis of specific criteria from the GPS data available on the NGL (`http://geodesy.unr.edu`).

In this chapter, the data processing procedures are illustrated step by step, starting from the outliers removal and offset correction and ending with the interpolation of the signals, in order to prepare the time series for the identification of dominant frequencies.

2.1 GPS data

For this study, the GPS data were acquired from an online data set (`http://geodesy.unr.edu/`), made available by the Nevada Geodetic Laboratory (NGL), which provides time series of coordinates of stations distributed all over the world.

The GPS data are analysed by the NGL using the GipsyX Version 1.0 software (Bertiger et al., 2020).

Models are adopted to correct the observations for effects, such as the ionospheric delay, the wet and dry tropospheric delay, the ocean and solid earth tides and solar radiation pressure.

This study analyses the Up component which describes vertical crustal displacements.

2.1.1 Selection of stations

The main purpose of this work is to identify and analyse periodic signals in the time series of the Up component of the GPS stations located in the European and Mediterranean area. The selection of the GPS stations is done on the basis of the length of the time series and considering a coverage as homogeneous as possible over the area of interest. Furthermore, the series shall be of good quality, this includes that they should be nearly continuous without major data interruptions.

Over the European/Mediterranean area, a rectangle has been selected within the following latitude ϕ and longitude λ ranges:

- $35° \leq \phi \leq 71°$
- $-24° \leq \lambda \leq 39°$

The time window identified is of about 18 years, from May 30, 2001 to the March 27, 2019.

The number of selected stations is 36 and they are shown in figure 2.1.

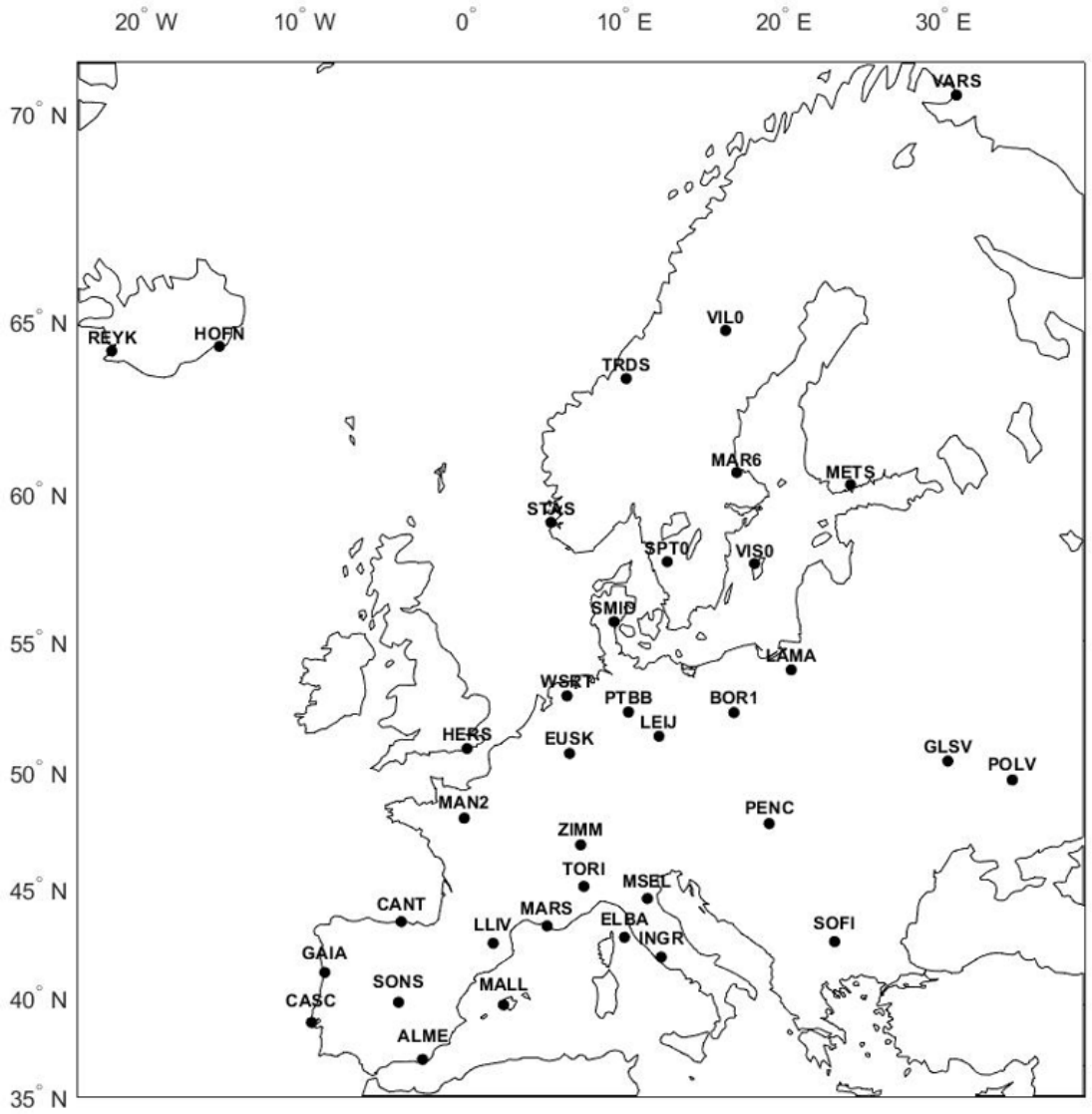

Figure 2.1: The selected network of GPS stations.

2.2 Outliers

The analysis of the Up time series may show the presence of a number of values that differ remarkably from the main trend of the time series. These values are known as outliers and their definition is not unique; the most common is the one given by Hawkins (1980):

> "An outlier is an observation that deviates so much from other observations as to arouse suspicious that is was generated by a different mechanism".

The main problem with this definition is the fact that it does not specify how the observations shall fit together.

In geodesy, the term outlier is defined on the basis of a statistical hypothesis test for the presence of gross measurement errors in the observations (Baarda, 1968; Pope, 1976; Heck, 1981). Observations that are rejected by such a test are called outliers.

The detection of outliers and the subsequent removal has many advantages, including the detection of outliers can be remeasured (Lehmann, 2013).

One of the most used criteria for identifying outliers is the 3σ rejection criterion, which is the one applied in this study. It considers outliers all the observations that deviate from the mean of an amount equal to or greater than three times the standard deviation.

The presence of outliers can be related to variations in GPS positional accuracy, which depends on different types of factors (Ordonez et al., 2011), such as:

- errors in the satellite and receiver clocks
- accuracy in the determination of atmospheric delays
- errors in satellites ephemerides
- satellite geometry

The procedure used in this work follows the rejection criterion mentioned above, considering time windows of 6 months. Firstly, a 2σ rejection was applied, secondly the 3σ one. The main reason to operate in this way is due to the

rather high level of noise present in the GPS time series. After applying this procedure, each single time series has been inspected and the remaining outliers were eliminated manually.

In figure 2.2 an example of the removal of outliers is shown. The blue dots are the clean data and the red ones are the outliers identified by applying the methodology described above.

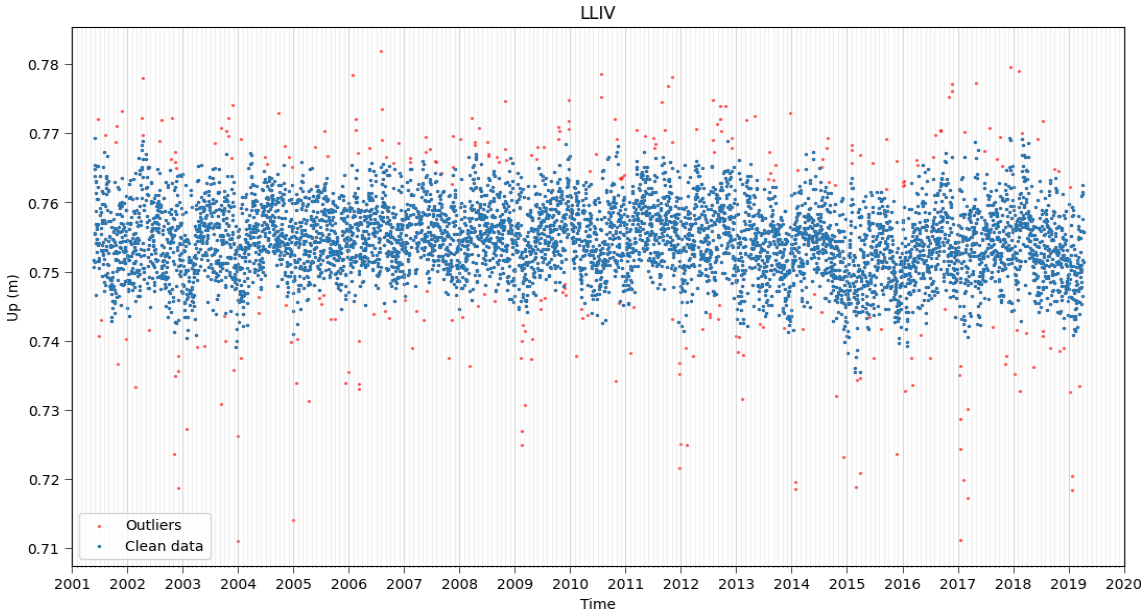

Figure 2.2: Time series of the Up coordinate of LLIV station (Spain); the red dots represent the outliers identified by the applied methodology, the blue dots show the final series, after removal of the outliers

2.3 Offsets

In general, the GPS Up coordinates time series are characterised by non-linear variations and, sometimes, by discontinuities which show up as sudden jumps. The latter are the so called offsets, which result in a sharp change of the mean resulting in a long-lasting effect on parameters. Undetected offsets may provide a detrimental effect on vertical motions of the stations and, in addition, as the length of the time series increases, the number of offsets is likely to increase, with the consequence that the cumulative effect of even small offsets can remarkably alter the estimation of positions and velocities (Gazeaux et al., 2013).

The detection of these discontinuities is a problem investigated in a large number of scientific studies, especially in geodesy, where their identification is

essential in order to perform a satisfying data processing.

Offset detection methods are essential for the removal of the effects that cause them, particularly in the case of those due to the unknown sources. The most common causes for these jumps are:

- seismic events;
- changes in the station equipment;
- multi-path;
- antenna problems;
- vandalism.

Gazeaux et al. (2013), analysing 340 GPS stations, found the statistics described in figure 2.3. This figure shows the percentages of the events that generate these sudden jumps, two thirds of which are known, while one third is related to unknown causes. The main difference between offsets with known and unknown cause is within their full width at half maximum, which is higher for jumps generated by equipment changes and seismic event offset, compared with the unknown ones. Therefore, the latter appear to be smaller than the others, making them more difficult to detect (Gazeaux et al., 2013).

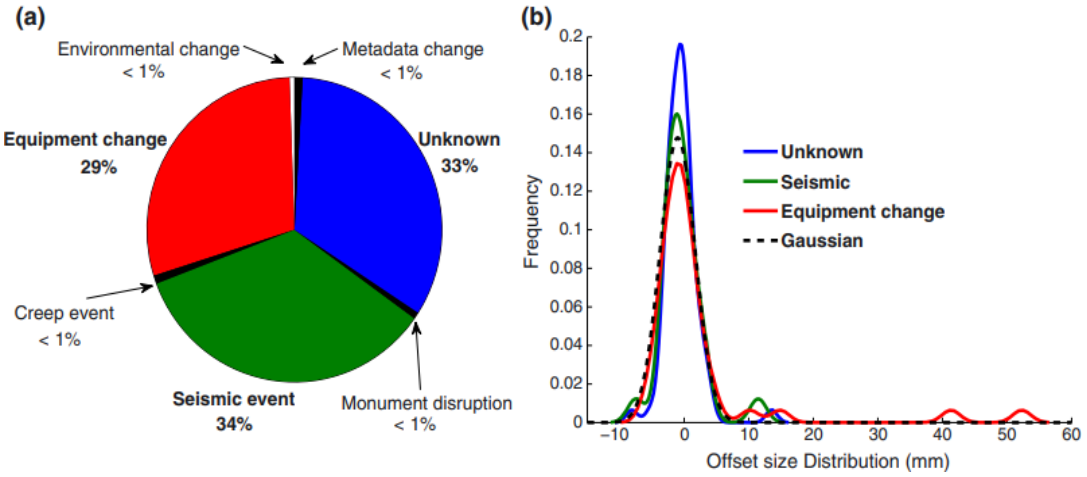

Figure 2.3: SOPAC offset description (a) and magnitude distribution (b) since 1995 over 340 sites (560 offsets)(Gazeaux et al., 2013).

The detection of offset was made in different steps during this work. First of all, for each singular station, the NGL indicates the known problems responsible

for the discontinuities and the relative day of happening. The main problem is that NGL only declares the ones caused by:

- Equipment changes: elevation cut off and antenna changes, receiver and model changes, random code changes;
- Earthquakes: A potential step record appears when this distance from this station to earthquake epicenter (in km) is less than $10^{\left(\frac{M}{2}-0.79\right)}$, where M is earthquake magnitude;
- Change of reference frame.

If the day of occurrence of the event is known, the procedure is applied following 3 steps: first, two windows, corresponding to all the data before and after the occurrence of the jump, are selected; second, for each of the two windows, a linear fit is estimated; third, at time t corresponding to the occurrence of the discontinuity, the difference between the two linear interpolations allows to identify the magnitude of the jump. This value is then added to all the data of the time series before the jump occurrence.

After removing all the reported offsets,an additional procedure was applied to identify possible discontinuities not reported by NGL. To do this, STARS algorithm (Bruni et al., 2014) was used to analyse the Up time series. It allows identifying both the epoch of occurrence and the magnitude of jumps corrupting the GNSS data sets without any prior information on the quantities (Bruni et al., 2014). The procedure is based on the Sequential t test Analysis of Regime Shifts (Rodionov, 2004).

An example of detection and removal of the offsets is shown in figure 2.4, where two discontinuities are clearly observable on August 19, 2010 and on June 28, 2013. Both are attributable to a change of the antenna code, as reported by NGL.

Figure 2.4: Example of offsets correction for the Up tie series of the METS station (Finland). Panel a) shows the original time series where two discontinuities can be recognised on August 19, 2010 and June 28, 2013. Panel b) presents the time series after removal of the two discontinuities.

2.4 Seasonal variations

The Up time series are usually affected by clear seasonal signals, which shall be modeled and removed so as to achieve the possibility to identify other signals characterised by oscillations of smaller amplitude.

The seasonal signal is mainly due to overlapping annual and semiannual periodicities. Many studies (Zou et al., 2015; Pan et al., 2016; Wang et al., 2017) have described the seasonal vertical deformation in terms of a loading mechanism exerted on the Earth's crust by different forces. Well known effects are those due to the atmosphere, the ocean and regional/local hydrology (M. Baldwin et al. 2001, 2002).

In this work a mean seasonal cycle has been estimated by stacking of the stations Up values. To obtain appropriate data to be used in the stacking procedure, the stations Up time series were first analysed to remove outliers and then detrended.

The GPS Up coordinate time series were analysed by the following procedure:

1 estimation and removal of the linear trend to obtain residual time series;

2 analysis of the residual series to identify possible interannual signals, which shall be removed by means of a suitable order polynomial;

3 generation of the mean annual cycle by stacking of the resulting residual series; removal of the estimated mean annual cycle.

Figure 2.5 shows an example of the results obtained adopting the procedures described above. It refers to the METS station, located near Helsinki, in Finland.

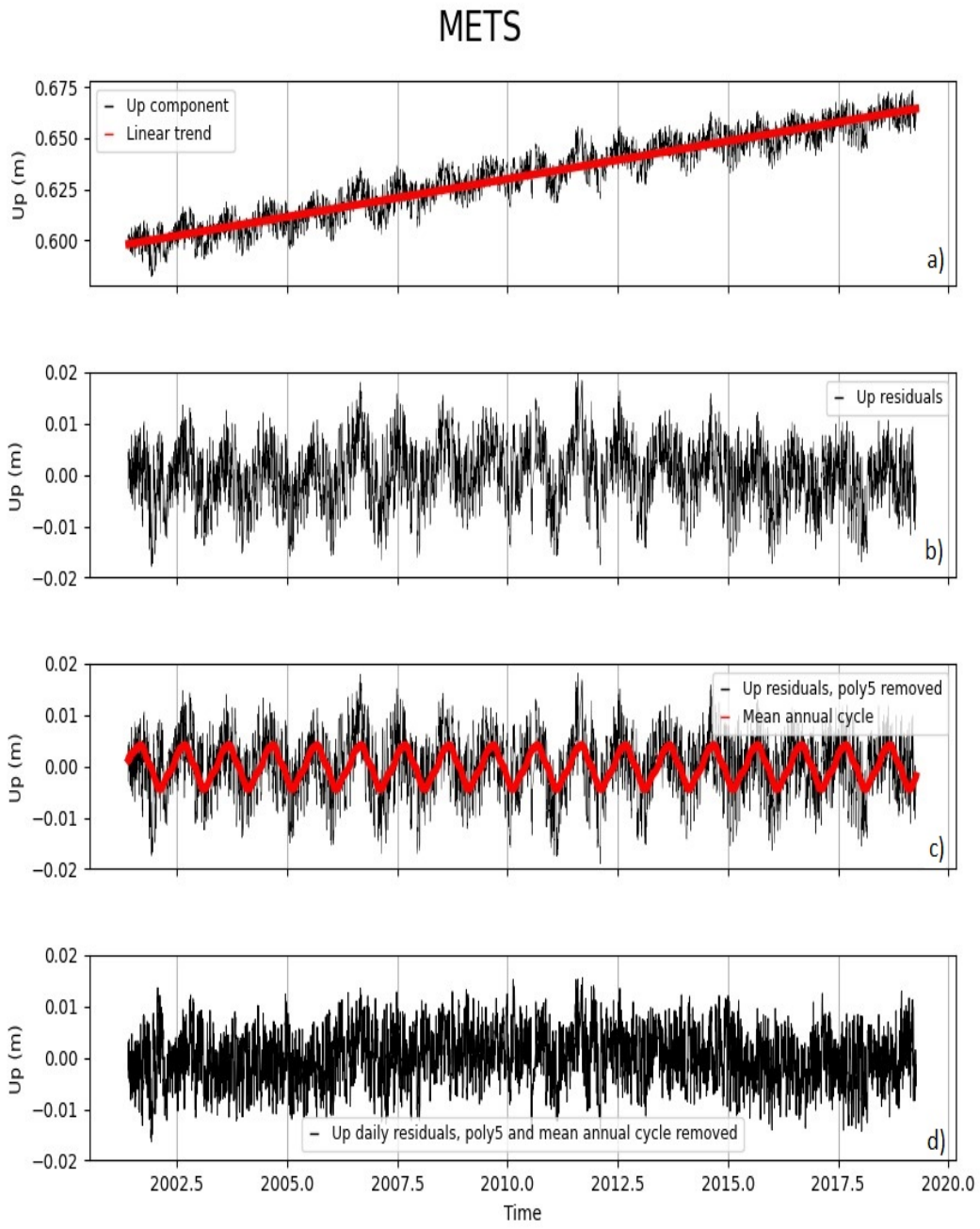

Figure 2.5: identification and removal of the seasonal cycle from Up time series; the example refers to the station METS in Finland. a) dayly time series of the Up component (black line) and estimated linear trend (red line); b) residual time series, where linear trend was removed; c) time series of residuals obtained after removing the estimated linear trend; c) residuals after removal of a 5^{th} order polynomial (black line) and the estimated mean annual cycle (red line); d) daily time series after removal of the linear trend, the 5^{th} order polynomial and the mean seasonal cycle.

2.5 Data fitting by cubic spline functions

A spline is a piecewise polynomial function, composed by polynomial defined in sub-intervals joined together with determined smoothness conditions (De Boor et al., 1978). The resulting curve has a continuous target, curvature and derivatives up to some specific order.

2.5.1 Mathematical description

Given a closed and limited interval $[a, b]$ and a partition Δ, defined as

$$\Delta = a = x_0 < ... < x_k < x_k < x_{k+1} = b \qquad ,$$

which induces a partition of $[a, b]$ in $k + 1$ intervals

$$\begin{array}{l} I_i = [x_i, x_{i+1}] \\ \qquad\qquad\qquad\qquad i = 0, ..., k-1 \qquad . \\ I_k = [x_k, x_{k+1}] \end{array}$$

Given a positive integer $m < k$, the following is the formal definition of a polynomial spline function of order m and of class C^{m-2}:

> **Definition** *A polynomial spline function of order m with nodes $x_1, ..., x_k$ of class C^{m-2} in $[a, b]$ is a function $s(x)$ that coincides in each sub-interval $I_i (i = 0, ..., k)$ with a polynomial $s_i(x)$ of order m and that, in the nodes $x_i (i = 1, ..., k)$, satisfies the continuity conditions:*
>
> $$\frac{d^j s_{i-1}(x_i)}{dx^j} = \frac{d^j s_i(x_i)}{dx^j} \qquad ,$$
>
> *with $i = 1, ..., k$ and $j = 0, ...m - 2$* (De Boor et al., 1978).

The space of polynomial spline of order m of class C^{m-2} in $[a, b]$ with nodes $x_1, ..., x_k$ is indicated by $S_m(\Delta)$, with dimension $m + k$. For each subinterval $I_i, (i = 0, k)$, the polynomial $s_i(x)$ of order m has m degrees of freedom, therefore there will be $(k+1)m$ degrees of freedom, from which the conditions of connection on each node have to be removed.

A good base for the spline space $S_m(\Delta, M)$ is the base of the normalised B-spline.

Definition *Given a succession of simple nodes* $... < x_1 < x_2 < ...$*, a normalised B-spline of order* m*, relative to the node* $x_i, N_{i,m}(x), x \in [a, b]$ *is a function with the following properties:*

- $N_{i,m}(x)$ *for* $x < x - i, x > x_{i+m}$ *(compact support);*
- $\int_{x_i}^{x_{i+m}} N_{i,m}(x)dx = \left(\frac{x_{i+m}-x_i}{m}\right)$ *(normalisation condition).*

In each interval I_j the normalised B-spline coincides with a polynomial of order m, with connects appropriately with the adjacent, so that $N_{i,m}(x) \in C^{m-2}[a, b]$ (De Boor et al., 1978).

In this work cubic spline functions are used to interpolate the data before proceeding with the Principal Component Analysis (see chapter 3). This method had been preferred to linear interpolation, due to the presence of a few large gaps in data sets (up to two months of missing data in a row), in order to obtain a better fit and a more realistic series.

This process, as mentioned before, consists in a series of unique cubic polynomials fitted between each point of the series, with the aim of obtaining a continuous and smooth curve (McKinley et al., 1998) (figure 2.6).

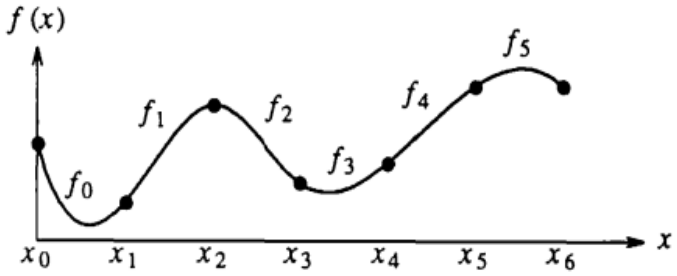

Figure 2.6: Example of cubic spline passing through n data points (Wolberg, 1988).

Spline functions are able to correlate data efficiently and effectively, regardless of the randomness of the data set.

Each time series was analysed in order to obtain the best possible fit by the selecting the appropriate number of splines necessary to fill the gaps.

The fitting method used in this study is the least squares cubic spline approximation, with a given set of fixed knots. As input to the Matlab function (`spap2`), in addition to the time series data, a specific value needs to be given, the positive integer l, which represents the number of polynomial pieces. The function returns the basis-form of a least-squares spline approximation, with the

knot sequence appropriately chosen. The resulting piecewise polynomial consists of l pieces and has m-2 continuous derivatives (m is the order of the spline, in this case it is 4 because a cubic spline had been used). In figure 2.7 and 2.8 it is shown an example of this application to the time series of station ALME (Spain), considering a spline function (k=3) with two polynomial pieced (l=2).

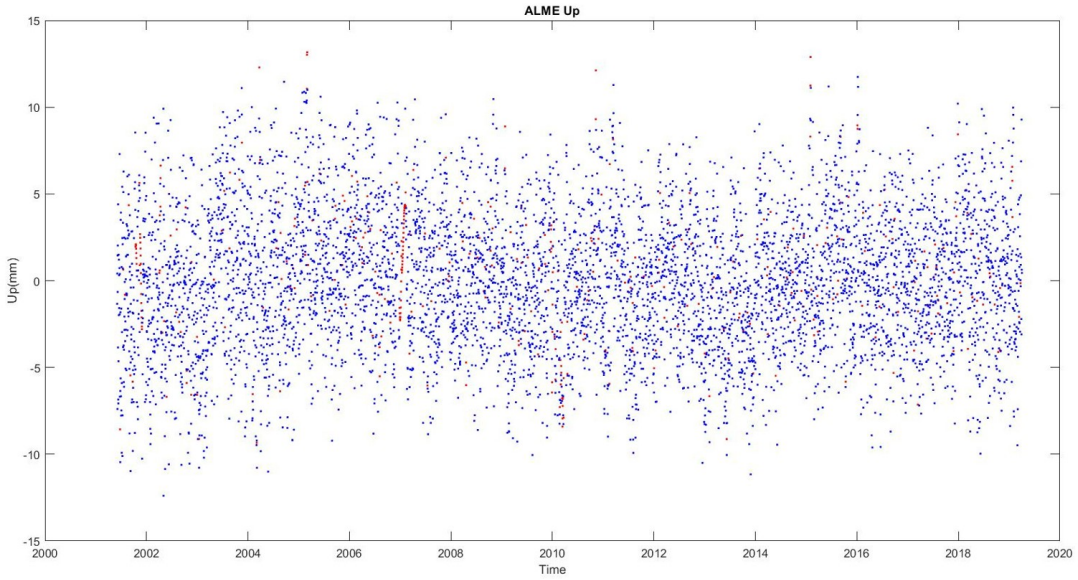

Figure 2.7: Spline interpolation of the data of station ALME (Spain). The blue dots are the data before the interpolation, while the red ones are the interpolated dots.

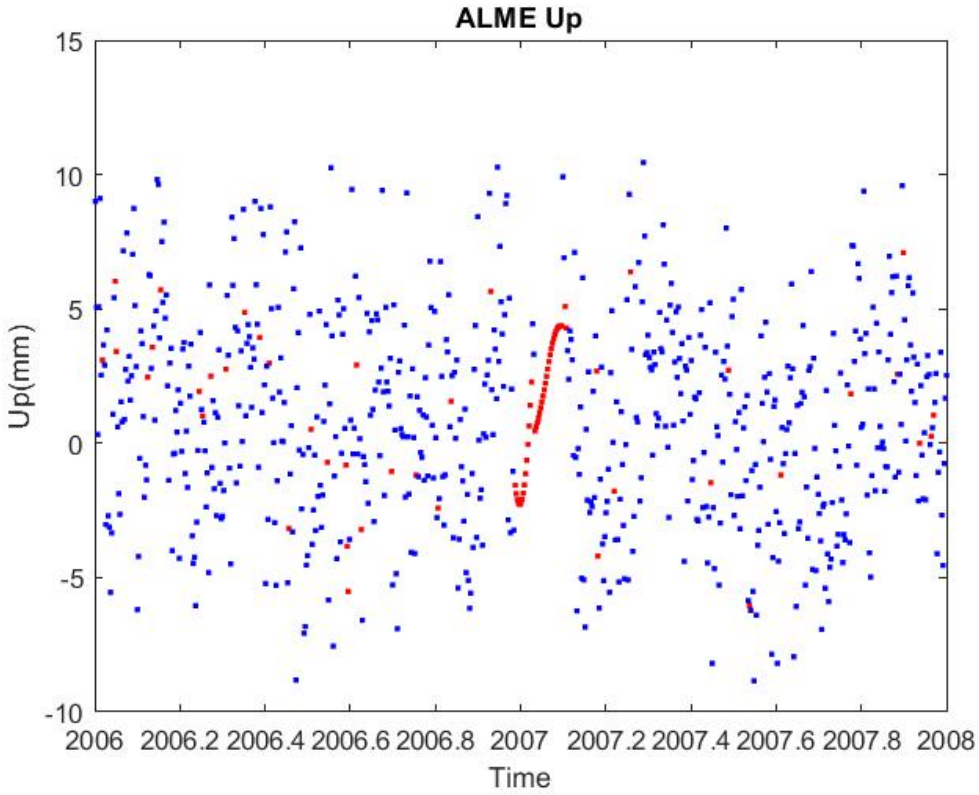

Figure 2.8: Details on the interpolation of the data of station ALME (Spain), between January 2006 and December 2007; the blue dots are the data before the interpolation, while the red ones are the interpolated dots.

The analysis performed using this procedure led to the elimination of three stations, ELBA (Italy), HOFN (Iceland) and VIL0 (Sweden), since they are characterized by too many missing data and the interpolation would have created unrealistic series.

After eliminating the stations mentioned above, the distribution of the stations is still homogeneous. Figure 2.9 shows the map of the area of interest and all the 32 stations that were retained after the data pre-processing of the data.

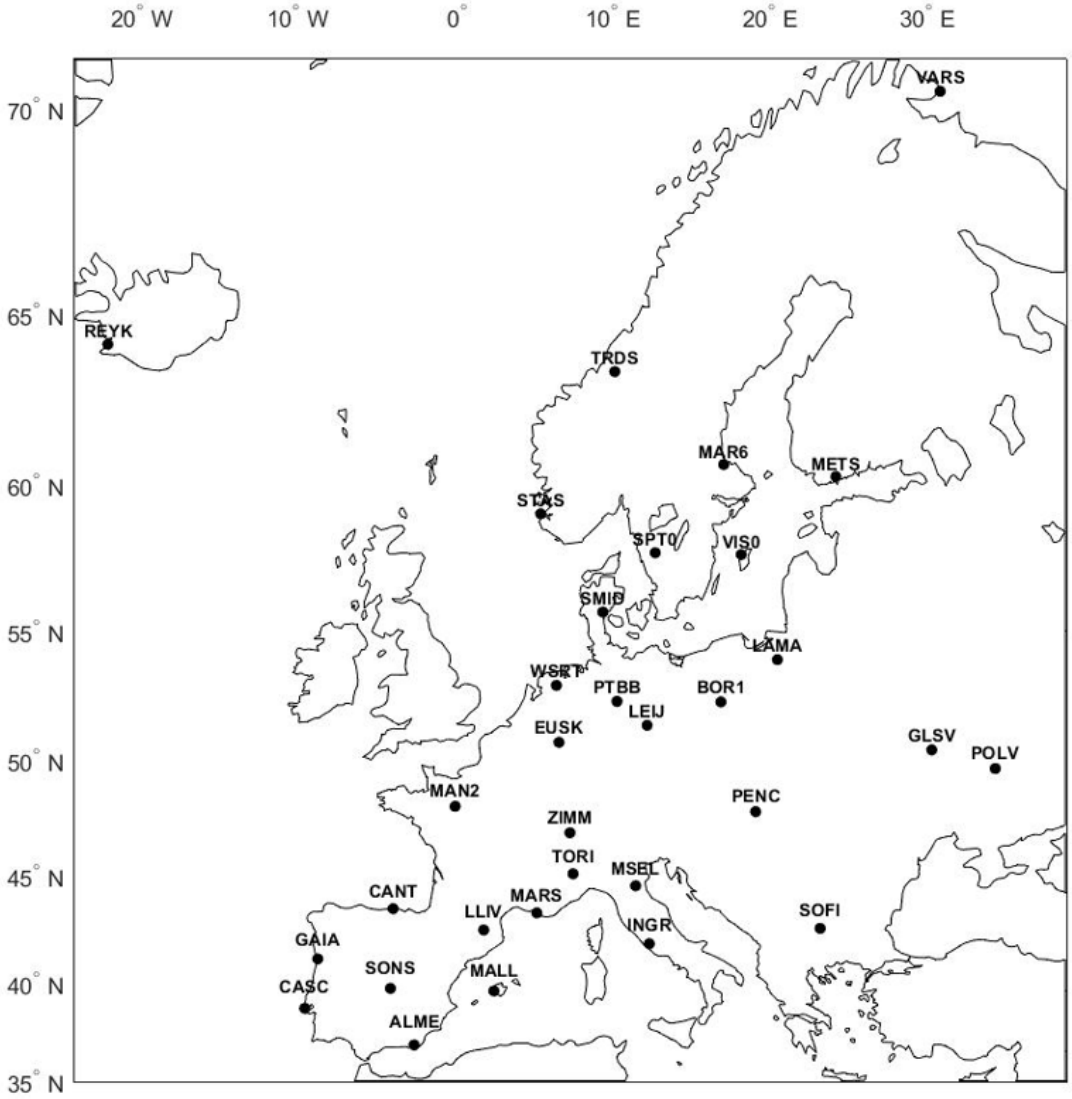

Figure 2.9: Network of stations after the pre-processing of the data.

Chapter 3

Principal Component Analysis (PCA)

The Principal Component Analysis (PCA) is a multivariate technique that enables the analysis of a data set in order to reduce its dimensionality, while preserving as much variability as possible (Jolliffe et al., 2016). The purpose is to extract information from the statistical data set to present it as a set of new orthogonal variables, called principal components, and to display the pattern of similarity between the observations and the variables as points in spot maps. It was first devised by Pearson, in 1901, and secondly developed independently by Hotelling in 1933.

From a mathematical point of view, PCA depends on the eigen-decomposition of positive semi-definite matrices and on the Singular Value Decomposition (SVD) of rectangular matrices. Eigenvectors and eigenvalues provide the eigen-decomposition of a matrix, which analyses the structure of it, such as correlation, covariance or cross product matrices (Mishra et al., 2017).

The main objective of this analysis is to reduce the dimensionality of the data set, considering the fact that most of the variables are interrelated. This reduction is achieved by transforming the data sets in a new one, composed by new variables (principal components PCs), which are not correlated, and which are ordered so that the first few retain most of the variability present in the original variables.

3.1 Mathematical definition

The first step to define the PCA is the organisation of the dataset in a matrix. It is assumed that the set is formed by measurements of the same variable, taken at p different positions and n different epochs:

- Positions $x_1, x_2, ..., x_p$;
- Epochs $t_1, t_2, ..., t_n$.

At each epoch, the measurements of the different positions constitute a map or a field. Then they are organised in a matrix F_{ij}, where i is related to the time and j to the space; consequently, the column j is the time series of the position x_j and the row i is the map at epoch t_i.

$$F_{ij} = \begin{bmatrix} f_{11} & f_{12} & \dots & f_{1p} \\ f_{21} & f_{22} & \dots & f_{2p} \\ f_{31} & \ddots & & \vdots \\ \vdots & & \ddots & \vdots \\ f_{n1} & f_{n2} & \dots & f_{np} \end{bmatrix} = \begin{bmatrix} f(t_1,x_1) & f(t_1,x_2) & \dots & f(t_1,x_p) \\ f(t_2,x_1) & f(t_2,x_2) & \dots & f(t_2,x_p) \\ f(t_3,x_1) & \ddots & & \vdots \\ \vdots & & \ddots & \vdots \\ f(t_n,x_1) & f(t_n,x_2) & \dots & f(t_n,x_p) \end{bmatrix} \quad . \quad (3.1)$$

Each column is then standardized in order to have columns with unit variance and avoid that time series with greater variability dominate over the others. Additionally, the sets are comparable and there is no problem related to the unit of measure.

The covariance matrix of F is realised by calculating $R = F^t F$ and by solving the eigenvalue problem:

$$RC = C\lambda \quad , \quad (3.2)$$

where Λ is a diagonal matrix formed by the eigenvalues λ_i of R:

$$\lambda = \begin{bmatrix} \lambda_1 & & \\ & \ddots & \\ & & \lambda_p \end{bmatrix} \quad (3.3)$$

and the c_i column vectors of C are the eigenvectors of R corresponding to the eigenvalues λ_i. It is important to notice that both Λ and C are of the size p by p. In addition, R is a symmetric square matrix, therefore C is orthogonal and its

inverse coincides with its transpose, namely $C^{-1} = C^t$ and it can be written as

$$R = C\lambda C^t \qquad . \tag{3.4}$$

The vectors c_i are called spatial patterns and they are orthogonal, that implies they are uncorrelated in space. At this point the eigenvalues are not ordered, so they are organised for growing λ_i in C, based on how much variance they explain, from the moment that the eigenvalues are the squared variance explained by the mode of variability. By plotting the EOF (Empirical Orthogonal Function), stationary oscillations are obtained and their evolution in time is described by:

$$\vec{a_1} = F\vec{c_i} \qquad , \tag{3.5}$$

where the vectors $\vec{a_i}$ are the time components and those are the projections of the maps in F. These are the principal component (PCs) time series.

In addition, from the equation 3.5 it is possible to derive:

$$F = \sum_{i=1}^{p} \vec{a}_i \vec{c}_i^T \qquad . \tag{3.6}$$

Spatial patterns are usually used to reconstruct a cleaner version of the data, truncating the sum at some $i = p' << p$; this procedure is the so called dimentionality reduction (Björnsson et al., 1997).

Each row of the matrix F can be seen as a map or as a vector for a point in p-dimensional space. All the points in this space are observations and if they are random they would be distributed as a blob in the space; otherwise, if there are regularities in the data, all the points would be arranged in clusters or along a defined direction.

3.2 Interpretation of PCA

The main aim of the method is to determine the orthonormal basis vectors e_m that maximise the projection of the vectors f_i along the basis vectors.

From the mathematical point of view, the problem is to maximise

$$\sum_{i=1}^{n} (e_m^T f_i)^2 = e_m F^T F e_m^T = e_m R e_m^T \qquad , \tag{3.7}$$

with $m = 1, ..., p$, under the condition

$$e_i^T e_j = \delta_{ij} \qquad . \tag{3.8}$$

Therefore, under this constrain, the equation becomes

$$\nabla(\vec{x}^T R\vec{x}) - \lambda\nabla(\vec{x}^T\vec{x}) = 0 \qquad , \tag{3.9}$$

where λ is a Lagrangian multiplier. It is now possible to rewrite the equation (1.14), after some manipulation, in the form

$$R\vec{x} = \lambda\vec{x} \qquad , \tag{3.10}$$

which represents the eigenvalue problem for R. The interpretation of this equation leads to the conclusion that the eigenvectors of R arise when exploring for a new coordinate system along the data regularities.

The symmetric matrix R, following the spectral representation theorem by Hilbert, can be decomposed into

$$R = \lambda_1 c_1 C_1^T + \lambda_2 c_2 C_2^T + ... + \lambda_p c_p C_p^T \qquad , \tag{3.11}$$

which explains the way to interpret the principal components. This means that the greater λ_i is, the better the related spatial pattern represents R. From this conclusion it is possible to truncate at $p' < p$, considering only those eigenvalues that represent a determined percentage, for example 90%:

$$\frac{\sum_{i=1}^{p'} \lambda_i}{Tr\Lambda} \leq 90\% \qquad . \tag{3.12}$$

3.3 PCA results

In the following section, the results of the principal component analysis applied to the GPS Up component of the stations network are shown. The PCA is the methodology adopted to extract the main patterns of the space/time variability of the surface vertical displacement. It allows to obtain the spatial pattern coefficients (figures 3.1, 3.3 and 3.5) and the time component series (figures 3.2, 3.4 and 3.6) used to detect the presence of long-period signals and their effects

on the area of interest.

The maps of the spatial pattern coefficients were created by assigning the proper value to the station point on the map (Elia et al., 2021).

The most relevant modes of variability are the first three ones, which explain the 91.44% of the total variability, as shown in table 3.1.

Modes	Percentage of variance explained
1	81.75
2	7.09
3	2.6

Table 3.1: Percentage of variance explained by the first three modes of variability of the data set.

The first spatial pattern (figure 3.1) shows a homogeneous behavior of the stations over most of the study area except for a few sites in South Western Spain. The red, orange and yellow stations are positively correlated, whereas the green ones are negatively correlated. A few stations in South Western Spain and REYK, in Iceland, show small or even negative correlation. The first time component (figure 3.2) presents a long decadal oscillation, with a maximum around 2010-2011. This time component explains 81.75% of the total variance, which is a large amount if compared to those of the other components (table 3.1).

The second spatial pattern (figure 3.3) shows a Southwest to Northeast gradient. The time component (figure 3.4) is characterized by a nearly decadal oscillation, as the first time component, but the maxima are in this case around 2008 and 2018 (figure 3.2). It explains 7.09% of the total variance, which is a much smaller percentage with respect to that of the first time component (table 3.1).

The third spatial pattern (figure 3.5) shows a homogeneous behavior in North and central Europe and in the Iberian Peninsula. These stations are characterized by negative correlation while the central Mediterranean shows null or slightly positive correlation. The time component (figure 3.6) shows a decadal oscillation with maxima during 2003 and 2013 with superimposed a shorter period oscillation of about 4-to-5 years from 2006 to 2011. This mode only account for 2.6% of the total variance (table 3.1).

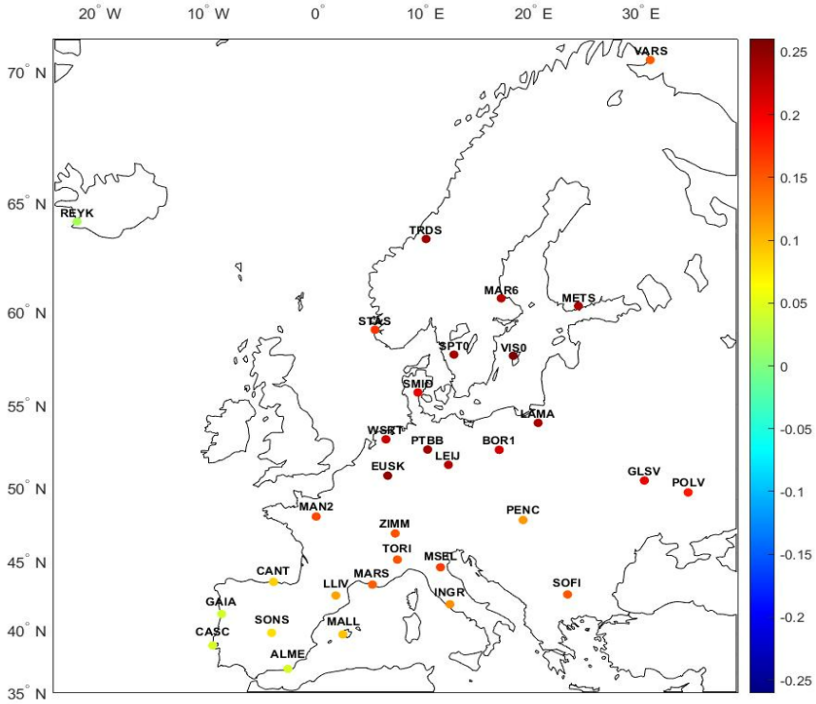

Figure 3.1: First spatial pattern of the GPS Up coordinate series. The percentage of variance explained is 81.75%.

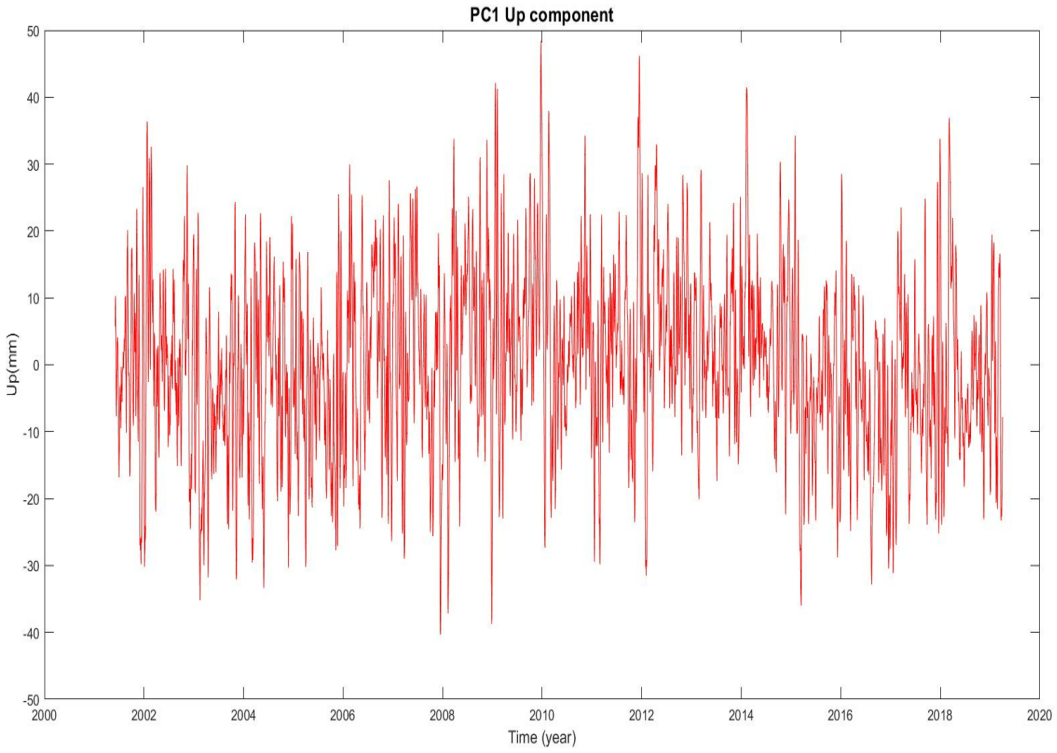

Figure 3.2: First time component of GPS Up coordinate series.

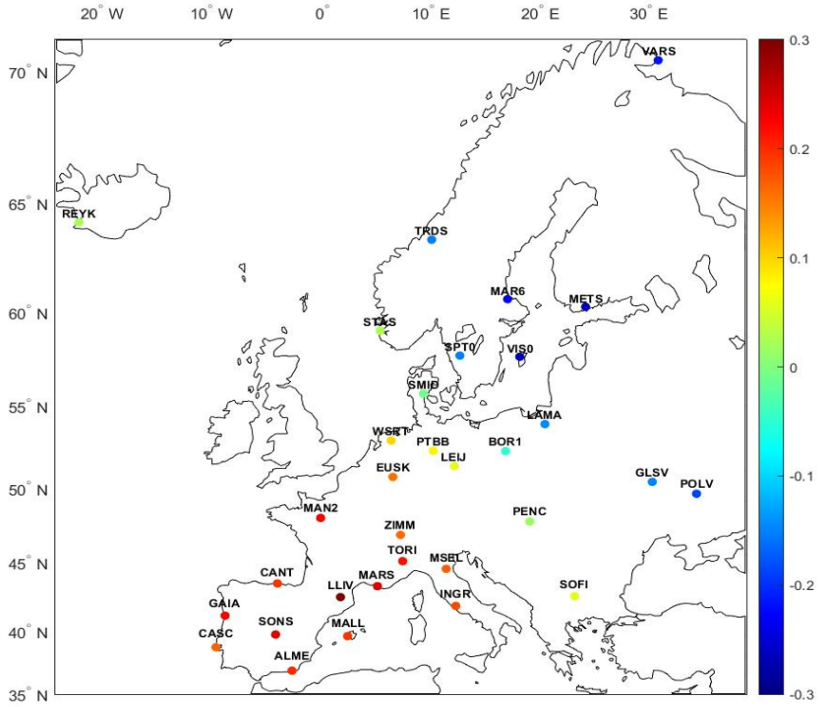

Figure 3.3: Second spatial pattern of the GPS Up coordinate series. The percentage of variance explained is 7.09%.

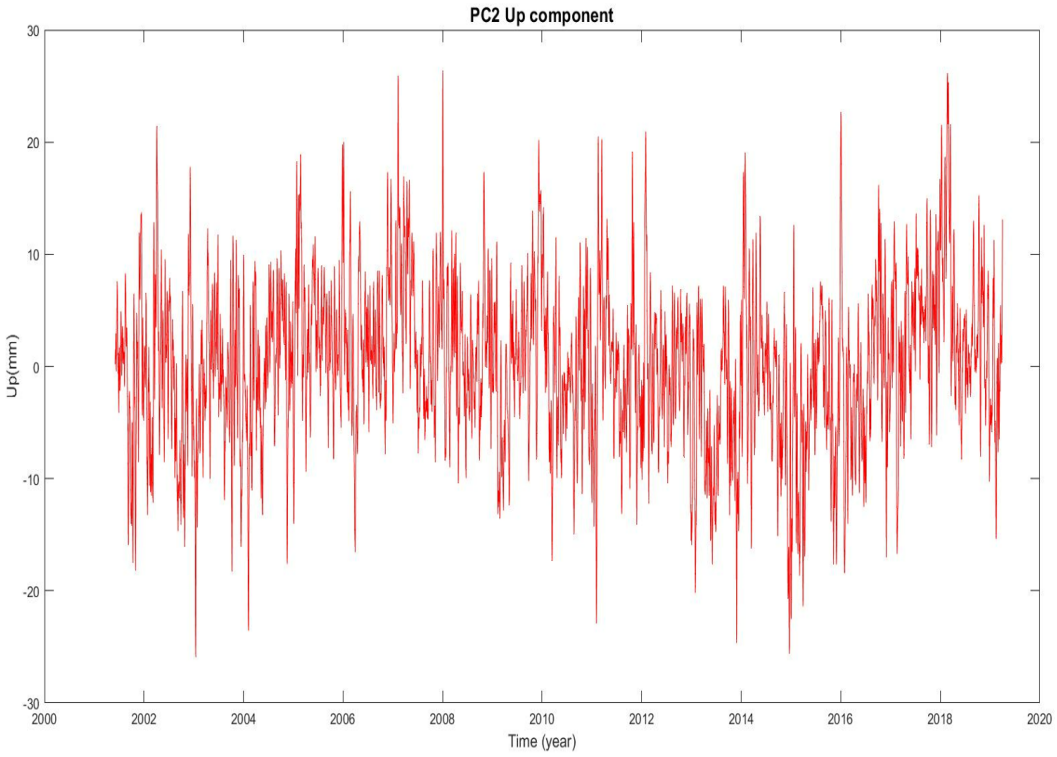

Figure 3.4: Second time component of GPS Up coordinate series.

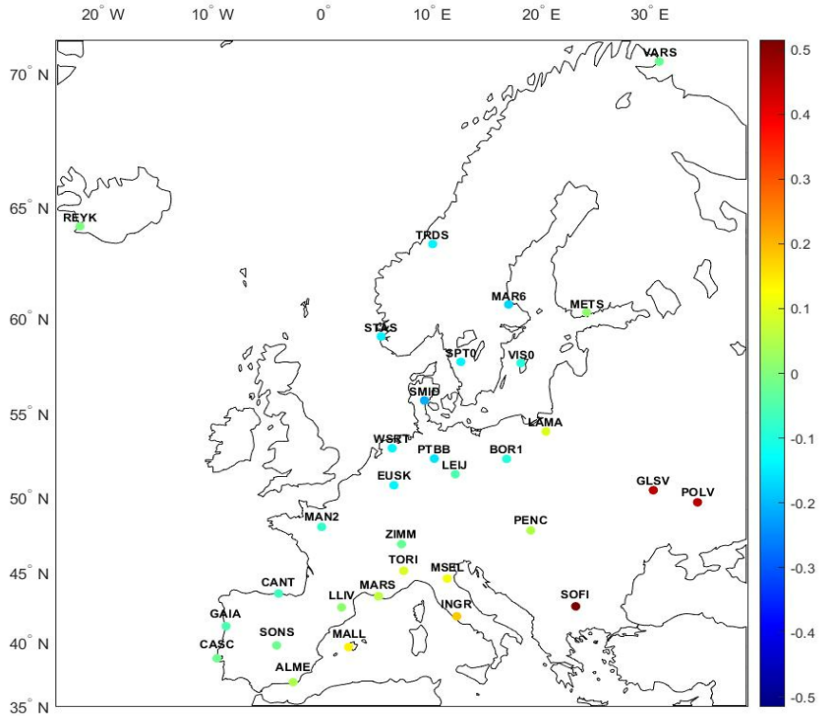

Figure 3.5: Third spatial pattern of the GPS Up coordinate series. The percentage of variance explained is 2.6%.

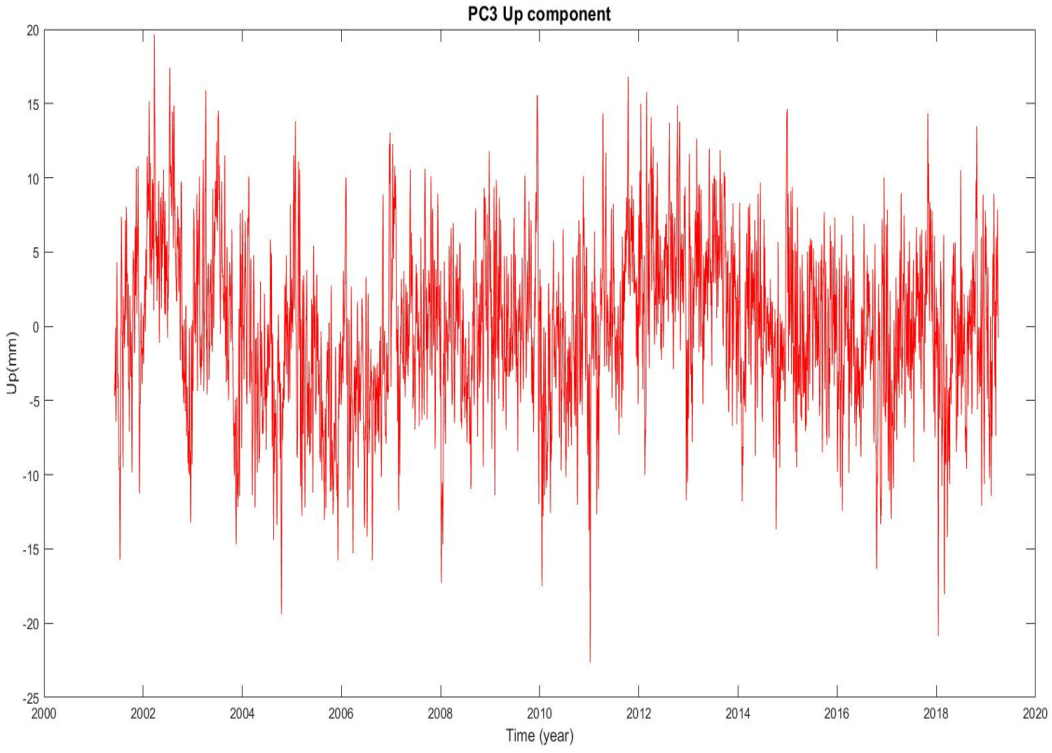

Figure 3.6: Third time component of GPS Up coordinate series.

Chapter 4

Frequency analysis

The methods chosen to identify possible frequencies of observed signals are the periodogram and the real-valued Morlet wavelet spectrum. This analysis provides the value and the magnitude of the frequencies, more specifically, the periodogram identifies the static frequencies of the signals, while the wavelet spectrum describes their behaviors in time.

4.1 Periodogram of PCA time component

In time series analysis, the periodogram is a diagram showing the most significant cyclical regularity in the data set. It allows to identify the dominant frequencies, or periods, of a time series, as an estimation of the spectral density of the signal. It describes a static behavior of the signals, therefore it was first used to identify the periodicities in the frequency domain. Then the wavelet transform, described in the next section, was applied to the PCA time component of the GPS Up coordinate series in order to describe the time behavior.

The main purpose of this work is to identify long-period oscillation signals. This means that the frequency domain to investigate is the one between zero and one cycle per year (cpy), corresponding to interannual (above two years) and interdecadal periods.

The periodogram of the first PCA time component of the GPS Up coordinate (figure 4.1 a) shows a frequency of 0.089 cpy corresponding to about 11 years and an amplitude of 14.01 mm. The following peak is due to a frequency of 0.1748 cpy corresponding to a period of about six years (5.72 years). The associated displacement of the GPS Up component is 3.16 mm. The following peaks are related to frequencies between 0.3 and 0.668 cpy corresponding to periods from two to four years.

The periodogram of the second time component of the GPS Up coordinate (figure 4.1 b) identifies a first peak (0.089 cpy) corresponding to about 11 years period, with a lower amplitude (7.70 mm) with respect to that found analysing the first time component. The oscillation with period of about six years causes a displacement of 3.94 mm in the GPS Up coordinate. Smaller peaks are also present in the frequency band 0.3-0.668 cpy, corresponding to periods of 2-to-4 years.

The periodogram of the third time component of the GPS Up coordinate (figure 4.1 c) shows a behavior similar to that of the previous time component (figure 4.1 b). The two main signatures are those corresponding to the about 11 and 6 years periods. The first one has an amplitude of 4.868 mm, while the second one of 3.31 mm.

Over the years of studying, interdecadal signals have been detected with periods above six years (Ding, 2019; Pan et al., 2019). It may seem that the periodogram can not reproduce low-frequency peaks below 0.15 cpy and the signals overlap with each others in the dominant peak at 0.089 cpy, preventing the obtaining of useful information. This means that some other low-frequencies may still exist in the GPS Up component time series, but they can not be identified. The length of the used record is not long enough to have an adequate frequency resolution, so the peaks of the longer period signals can not be isolated from each other.

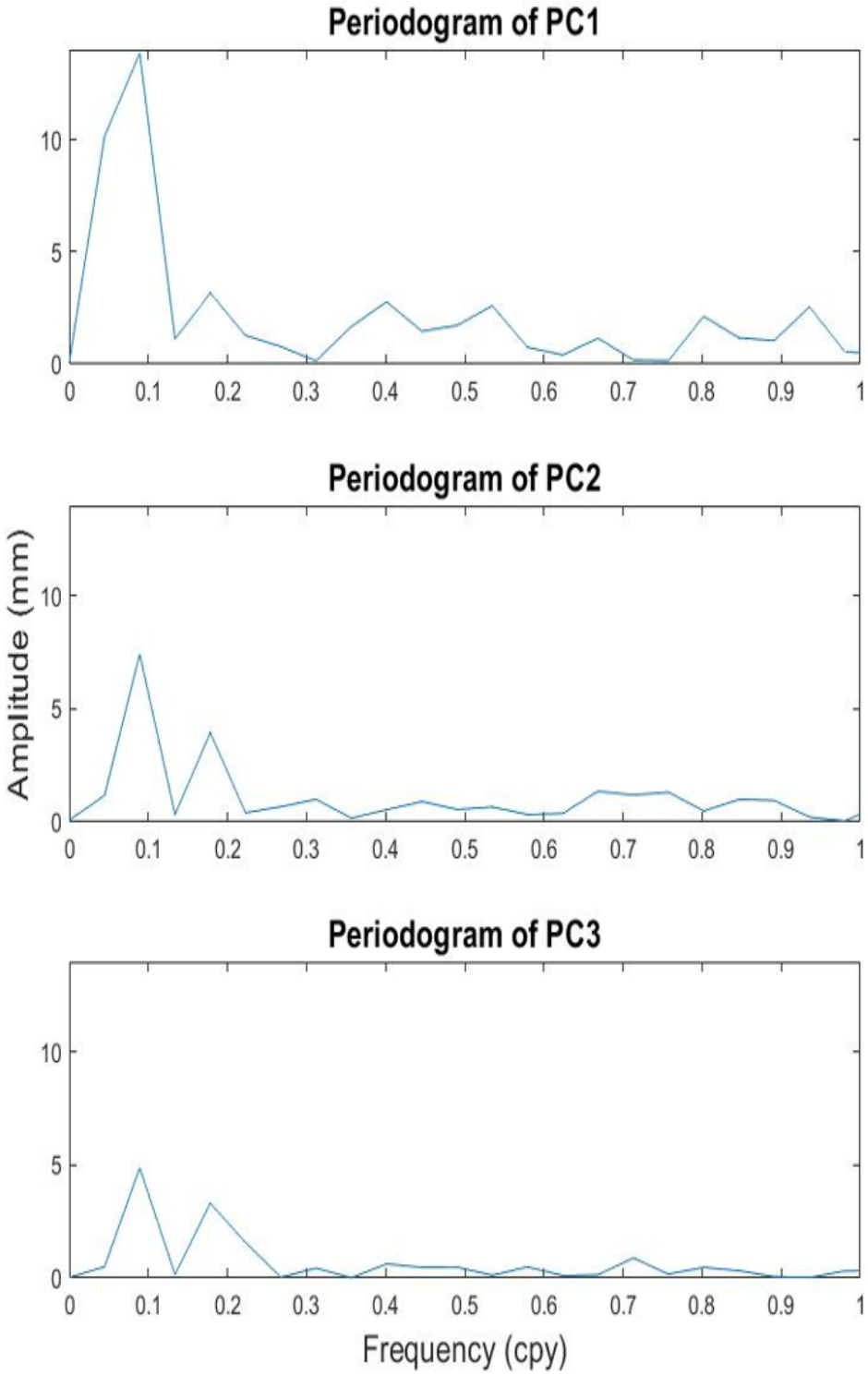

Figure 4.1: Periodograms of the first three principal component of GPS Up coordinate in the frequency band 0-to-1 cpy.

4.2 Continuous Wavelet Transform analysis

Continuous wavelet transform (CWT) were first introduced by the geophysicist Jean Morlet to propose a new method of the time-frequency analysis.

The theory beyond CWT is based on the Gabor wavelet, a sinusoidally-modulated Gaussian function, and the Heisenberg uncertainty principle to keep constant the product of the time and frequency widths of the wavelet (Russell et al., 2016). By analogy to the Heisenberg uncertainty principle, the Gabor uncertainty principle stated that spectral components can not be defined exactly at any instant in time (Gabor, 1946), therefore, it was not possible to have both a high-localization in timing or frequency content. On the other hand, the CWT varies in time length of its analysis window in order to achieve a varying time-frequency localisation. It uses long wavelets to interpret low frequencies precisely at the expense of limited time localization, and conversely short wavelets to ensure high time localization but limited information on frequency content (Rioul et al., 1991; Kumar et al., 1997).

The ultimate mathematical formulation of the CWT is:

$$S_W(\tau, a) = \frac{1}{\sqrt{a}} \int_{-\infty}^{+\infty} S(t) \overline{\Psi} \left(\frac{t-\tau}{a} \right) dt \qquad , \tag{4.1}$$

where $a \in \overline{\mathbb{R}}^+$ and $b \in \mathbb{R}$ are, respectively, the scale and the translational values and $S(t)$ is the signal. In this work real-valued Morlet wavelets are used for time-frequency analysis of non-stationary PCA time series. These type of wavelets are composed of a complex exponential multiplied by a Gaussian window and are defined by the *mother wavelet* function Ψ_σ(t):

$$\Psi_\sigma(t) = c_\sigma \pi^{-\frac{1}{4}} e^{\frac{-t^2}{2}} \left(e^{-i\omega_0 t} - e^{-\frac{\omega_0^2}{2}} \right) \qquad , \tag{4.2}$$

where c_σ is the normalisation constant and $\omega_0 = \sqrt{\frac{2}{ln(2)}}$.

This flexible scheme enables the CWT to be used for the analysis of a wide range of signals. Furthermore, the CWT is reversible such that signal reconstruction can occur after filtering or manipulating wavelet coefficients (Tary et al., 2018).

4.2.1 Denoising wavelet by Soft-Thresholding method

Before using the real-valued Morlet wavelet spectrum, a denoising procedure had been applied to each principal time component of the GPS Up coordinate series in order to smooth the high frequency signals without affecting the lower one. Therefore, wavelet spectrum highlights in a better way long-period oscillation.

The denoising by Soft-Thresholding method was proposed by Donoho in 1994. Given the ideal signal g, with dimension n, and the acquired signal $f = g+\epsilon$, where ϵ is the white noise, a vector long n obtained from a normal distribution with null mean and assigned variance, the wavelet denoising consist on the reconstruction of a good approximation $\hat{g}$ of g by minimising the following functional the following functional:

$$\hat{g} = arg\left(min_g \frac{1}{2} ||f - g|\,|^2 + \lambda||Wg||_1\right) \quad , \tag{4.3}$$

where the first term represents the fidelity term, which requires that g has to be faithful to f, the last one, the sparsity term, is a constrain on the sparsity of the wavelet coefficients and W is the orthogonal wavelet transform operator.

According to Donoho and Johnstone, the approximate solution of problem (4.3) is:

$$\hat{g} = W^T(\text{soft}_\lambda(Wg)) \quad , \tag{4.4}$$

with $\lambda = \sigma\sqrt{2ln(n)}$, where σ is the noise level and soft is the *soft threshold* operator:

$$\text{soft}(t) = \begin{cases} \text{sign}(x(t))(|x(t)| - \lambda), & |x(t)| > \lambda \\ 0, & |x(t)| \leq \lambda \end{cases} \quad . \tag{4.5}$$

An implemented example of the application of the soft threshold operator on a generic signal x(t) is shown in figure 4.2. The points of the signal between $[+\lambda, -\lambda]$ are eliminated; from the points $>\lambda$ the value λ is subtracted, from the points $<\lambda$ the value λ is added.

In figures 4.3, 4.4 and 4.5 are shown the time series of the first three principal components before (right) and after (left) the application of the denoising wavelet.

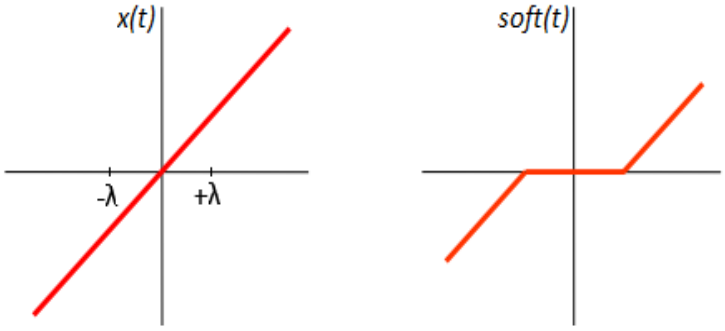

Figure 4.2: Implemented example of the application of the soft threshold operator.

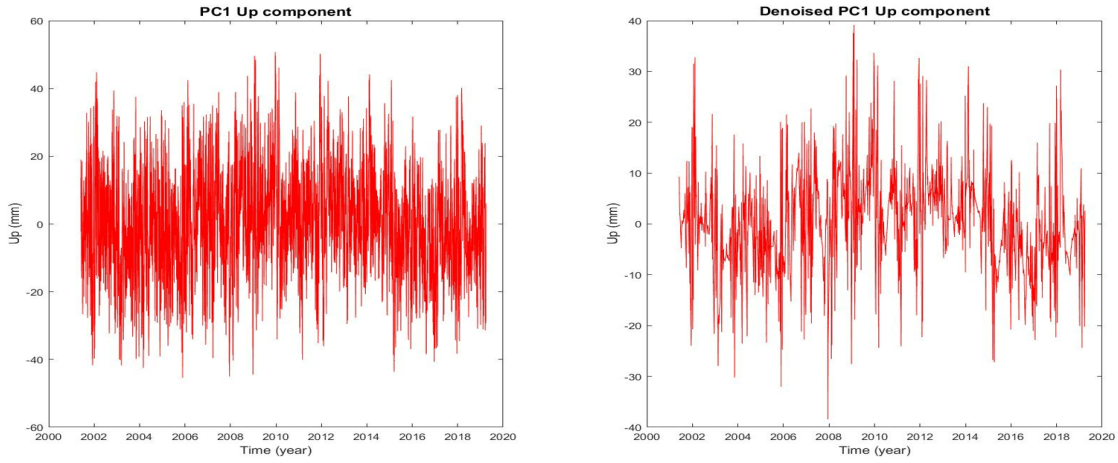

Figure 4.3: First time component of GPS Up coordinate before (right) and after (left) the application of the denoising wavelet.

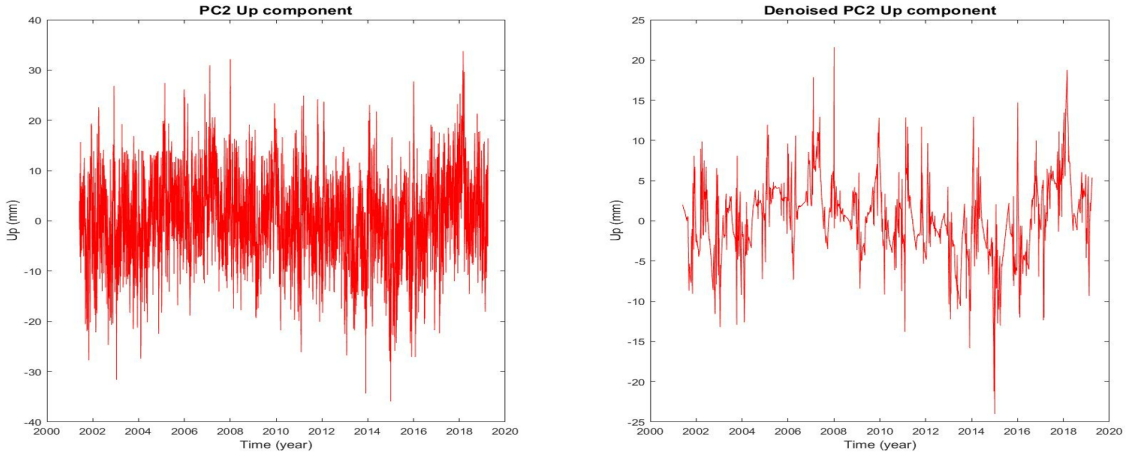

Figure 4.4: Second time component of GPS Up coordinate before (right) and after (left) the application of the denoising wavelet.

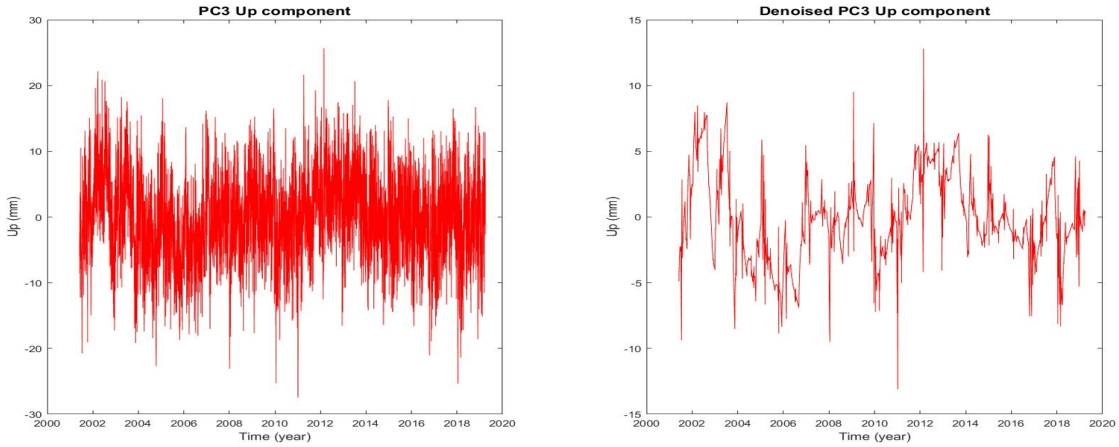

Figure 4.5: Third time component of GPS Up coordinate before (right) and after (left) the application of the denoising wavelet.

4.2.2 Morlet wavelet spectrum on denoised PCA

In this work real-valued Morlet wavelet are used for time-frequency analysis of non-stationary PCA time series. The main limitation of the periodogram (section 4.1) is the impossibility to describe periodic oscillations in time, while wavelet transforms are able to accomplish this task.

The wavelet spectra were obtained by choosing a number of scales equal to 43 in order to be able to investigate long periods and a spacing between scales of 0.1. The number of scales is correlated with the periods, therefore to analyse lower periods, less scales are needed. The colorbar indicated phases of oscillation of the signals; the red, orange and yellow bands represent a positive phase, the blue ones represent a negative phase.

The first principal component wavelet spectrum shows the dominance of a signal with a period of 18.6 years. It occurs exactly one time in the sampling interval of time from 2001 to 2019 (figure 4.6). There are two other signals with a much lower intensity appearing in the graph, respectively with period of $\sim$ 8-9 and $\sim$ 5.8 years. Analysing the lowest part of the spectrum, it is possible to notice the presence of signals with period between 2 and 4 years, which have been previously identified in the periodograms of figure 4.1.

The second principal component wavelet spectrum (figure 4.7) identifies the dominant signal at 18.6 years. The oscillations with period of 8-9 and $\sim$ 6 years are more evident respect to the ones recognised in figure 4.2.

The third principal component wavelet spectrum (figure 4.8) shows a similar

behavior with respect to the second one. The signal with a period of about 8-9 years and the ones with a period between 2 to 4 years are more evident with respect to the first two principal components.

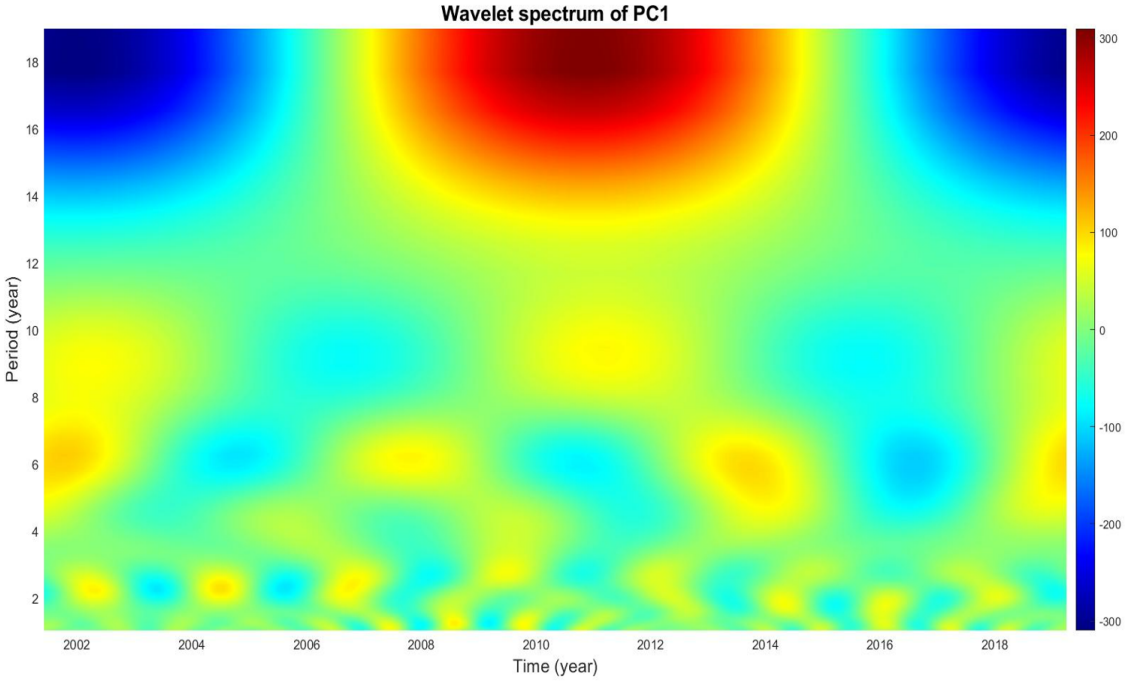

Figure 4.6: Wavelet spectrum of the first time component of the GPS Up coordinate series. The red and blue areas represent the polarity of the wavelet transform, respectively the positive and negative phases of the oscillation.

The main evident difference between the results obtained with the periodogram and with the wavelet transform appears in the signals with a period greater than 6 years. All the periodograms of the three principal components show only one peak between 0 to 0.1748 cpy, which represents a signal of about 11 years. The wavelet transform is a much more efficient method to investigate the frequencies (therefore the periods) than the periodogram. It is able to detect more periods, such as the ones related to signals of 8-to-9 and 18.6 years. It may appears that the first peak in the periodograms collects all these information that, instead, stand out in the wavelet spectrum, as previously supposed.

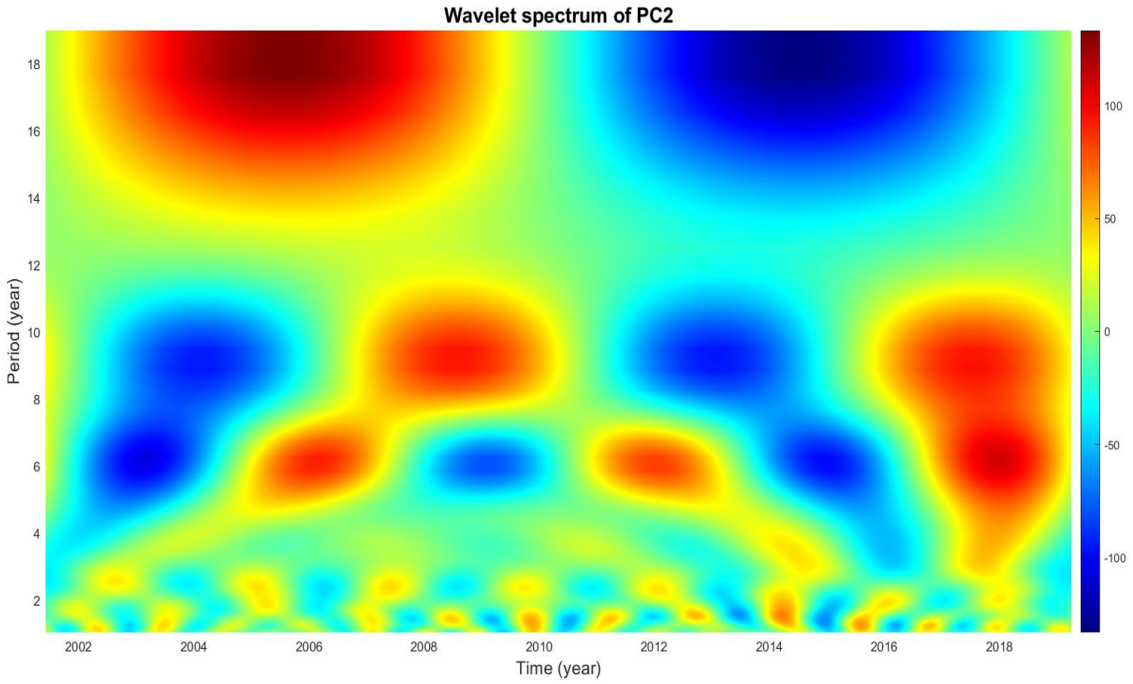

Figure 4.7: Wavelet spectrum of the second time component of the GPS Up coordinate series. The red and blue areas represent the polarity of the wavelet transform, respectively the positive and negative phases of the oscillation.

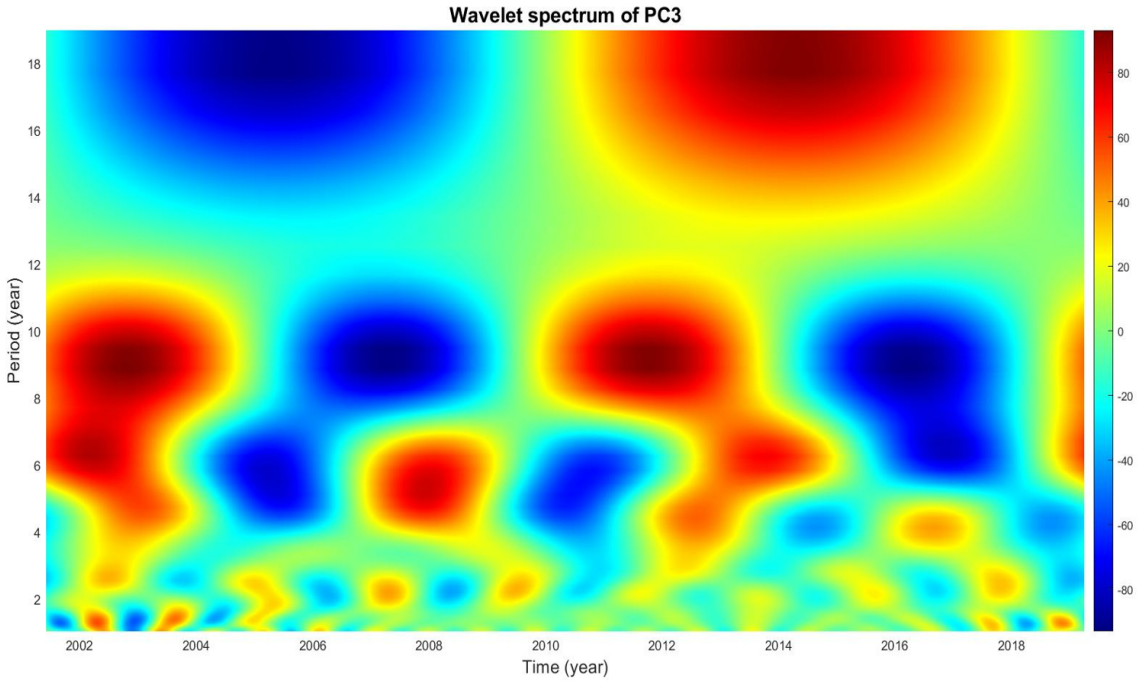

Figure 4.8: Wavelet spectrum of the third time component of the GPS Up coordinate series. The red and blue areas represent the polarity of the wavelet transform, respectively the positive and negative phases of the oscillation.

Chapter 5

Interannual phenomena in time series

The Earth's surface is subjected to deformations due to a number of geophysical and geological processes. Vertical motions are typically an order of magnitude smaller than the horizontal deformation (Teixell et al., 2009). Moreover, the GPS vertical coordinates accuracy, caused by the satellite geometry (e.g. Soycan et al., 2011) and systematic effects, is about half of the horizontal accuracy, due to inappropriately modelled tropospheric delay, antenna phase center variations or different loading processes (e.g. vanDam et al., 1994, Dam et al., 2001 and Boehm et al., 2004). Therefore, the identification and description of the nature of vertical deformations has always been challenging.

GPS time series are characterised by the superposition of interannual and interdecadal variations (Chapter Introduction). The mechanisms behind these fluctuations still need to be clearly understood.

In this chapter, the main interannual, regional and global phenomena that contribute to time series coordinates variability are described.

5.1 El Niño/Southern Oscillation (ENSO)

The dominant interannual variability of the climate system is ENSO, which plays a central role in seasonal to decadal climate prediction (Lin et al., 2019). ENSO is a climatic periodic phenomenon with variable period from 2-to-7 years including warming of the sea surface temperature (SST) across the equatorial Pacific ocean (NOAA CPC, 2020d). Nevertheless, ENSO effects are also reported to be relevant in Central and Eastern Europe (Bartholy et al., 2006; Shaman et al., 2011).

ENSO is defined by three different phases; two opposite phases, El Niño and La Niña, which require changes in both the ocean and atmosphere, and the neutral phase:

- *El Niño phase* causes a warming of the ocean surface, or above-average SST. The low-level surface winds, which normally blow from east-to-west, experience a weakening which causes a warming of the equatorial East Pacific and a cooling of the West Pacific (figure 5.1 b);
- *La Niña phase* causes a cooling of the ocean surface, or below-average SST. The winds become stronger and the equatorial East Pacific becomes cooler and the West Pacific becomes warmer (figure 5.1 a);
- *Neutral phase* occurs when neither El Niño or La Niña are manifesting.

ENSO produces a shift in basic climatological parameters, such as temperature or rainfall over Europe (Ineson et al., 2009). It plays a major role in large-scale variations in precipitation, which deform the Earth's surface through loadings effects.

5.2 Quasi-Biennial Oscillations (QBO)

The Quasi-Biennial Oscillation is a well known phenomenon, identified long before ENSO (Reed, 1961; Ebdon et al., 1961), that dominates the variability of the equatorial stratosphere (16-50 km) and it is seen as downward propagating easterly and westerly wind regime, with a variable period averaging approximately 28 months. Although it is a tropical phenomenon, it affects the stratospheric flow from pole to pole by modulating the effects of extratropical waves (M. Baldwin et al., 2001). According to Asbaghi et al. 2017, who analysed the tropospheric impact of QBO on the strength and position of North Atlantic and Mediterranean storm tracks by using the Freie Universität Berlin (FUB) radiosonde network data (`https://www.geo.fu-berlin.de/en/met/ag/strat/produkte/qbo/`), the impact of the QBO is more marked in late winter on the North Atlantic area, while it manifests in early winter in the Mediterranean area.

The QBO effects are found to be relevant in the observations of ionospheric total electron content (Tang et al., 2014), which can have effects on the GPS signal and, in addition, it has an impact on the surface weather and can be connected

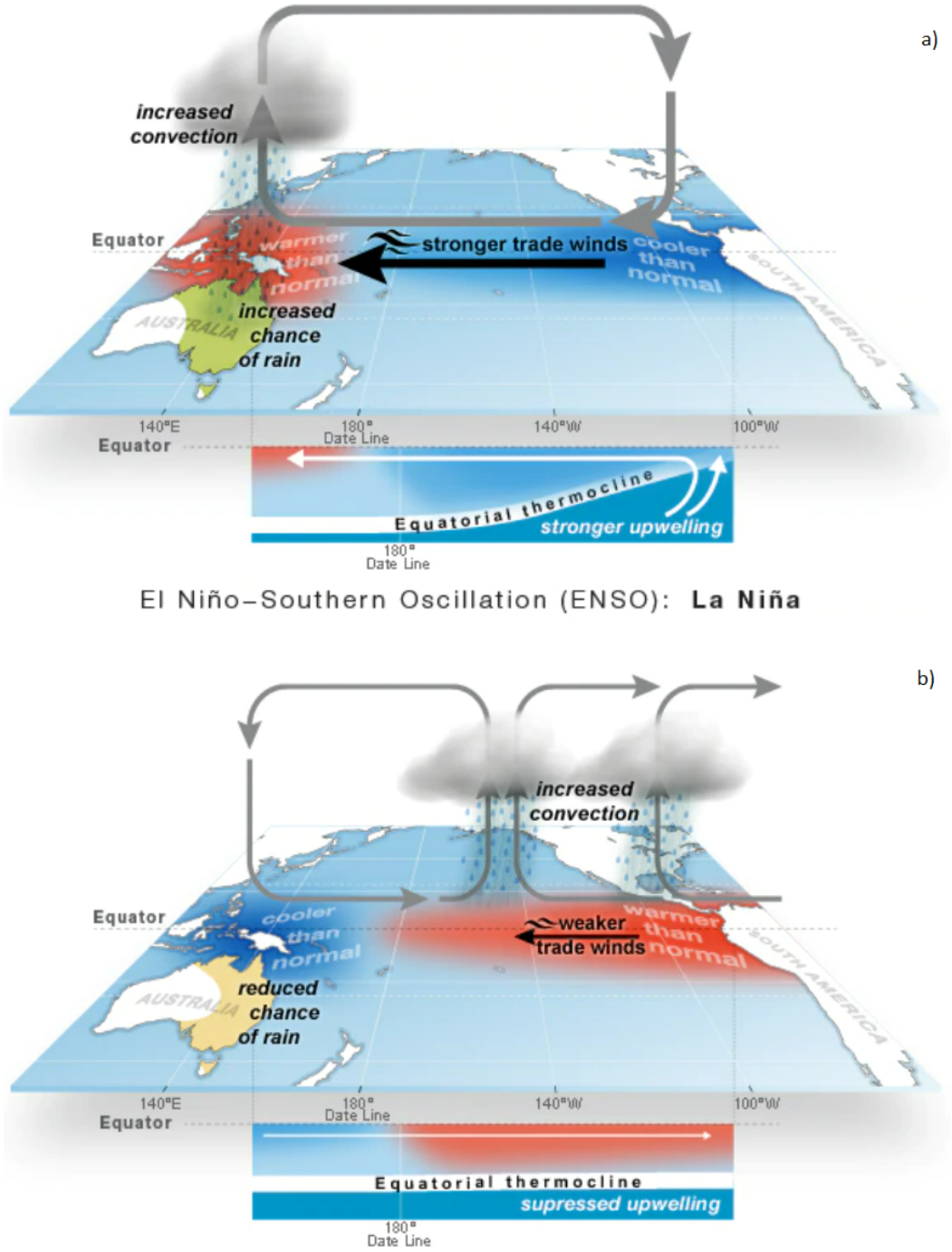

Figure 5.1: Representation of La Niña (a) and El Niño (b) (Doyle, 2018); red and blue colors indicate respectively higher and lower SST.

with the rainfall distribution that causes variations in the GPS heights through loading mechanisms (Asbaghi et al., 2017; Pan et al., 2015).

It is significant to consider the QBO signals in the GPS records to improve the

understanding of vertical deformations and vertical velocity (Pan et al., 2015).

5.3 Six (SYO) and Eight (EYO) year oscillations

Two periodic signals have been detected in the intradecadal period band, an approximately SYO (Abarca del Rio et al., 2000) and an approximately EYO (Ding, 2019; Duan et al., 2020). It has been argued that these signals might results from core-mantle interactions and core dynamics and that both SYO and EYO might be related to the short-period secular variations in the core geomagnetic field (Liao et al., 1999; Mound et al., 2006; Ding et al., 2021).

The SYO is an intradecadal oscillation firstly detected by Vondrak in 1997 by analysing the difference between the rotational time *UT1* and the atomic time scale *AT* over the period 1958-1969. It was confirmed by Liao et al. (1999) who studied the atmospheric angular momentum (AAM) monthly series from 1968 to 1997.5 provided by the NCEP (National Centers for Environmental Prediction) and the LOD series. They found an about 5.6 years oscillation (figure 5.2) and a peak-to-peak amplitude of about 0.3 ms in the residuals suggesting that the ΔLOD were excited by other geophysical processes rather than the atmospheric excitation, which resulted too small on the decadal time scale. On the interannual time scale, atmospheric processes, i.e. El Niño/Southern Oscillation (ENSO) and the Quasi-Biennal Oscillation (QBO), tend to dominate the excitation of ΔLOD (Chao, 1988; Chao, 1989). On the decadal time scale, several studies (Stix et al., 1984; Björnsson et al., 1997; Hinderer et al., 1990; Hide et al., 1991; Greiner-Mai, 1993; R. Holme, 1998) stated that the excitation of the ΔLOD was likely caused by the coupling between the core and the mantle.

Abarca del Rio et al. (2000), obtained the same results of Liao and Greiner-Mai by analysing AAM and LOD series from 1949 to 1998. They identified three different signals: a quasi-biennial, a triennial-quadrennial and one at six-seven years. The atmosphere appears to excite the first two oscillations, while it does not contribute to the last. This latter was found to be absent in the AAM records, therefore they stated that it was likely to arise from the interaction between mantle and core.

Mound et al. (2003), proposed a theoretical model of the core-mantle system

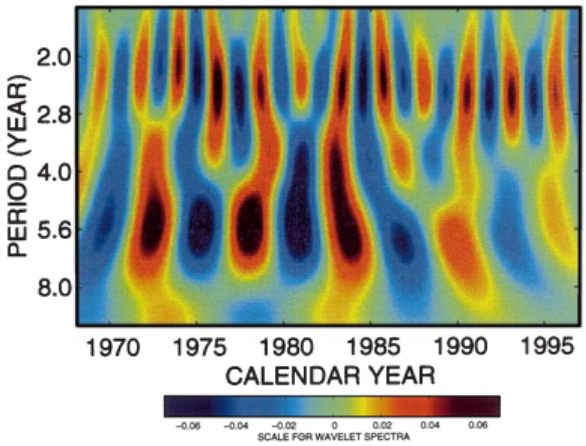

Figure 5.2: Wavelet spectrum for ΔLOD showing a clear dominant oscillation of about 5.6 years (from Liao et al., 1999).

that includes a combination of gravitational and electromagnetic couplings which allows angular momentum to be transferred between the solid inner core, fluid outer core, and mantle of the Earth. It allows to calculate the natural period of interannual oscillations in the axial rotation of the core and mantle.

The motion of the mantle and inner core are described by rigid body rotations. Convective motion in the mantle induces deformation of the core-mantle boundary (CMB) with a relatively large degree 2, order 2 surface spherical harmonic component (Forte et al., 1994; Defraigne et al., 1996), therefore the equatorial cross section of the CMB is elliptical. When the inner core boundary (ICB), which is also an ellipse in equatorial cross section, is in equilibrium, its axis and those of the CMB are aligned (figure 5.3 a). The fluctuation in the geodynamo process produce varying torques on the inner core that act to rotate it respect to the mantle (Glatzmaier et al., 1996; Buffett et al., 2000). As a consequence, the inner core shape relaxes to reduce the displacement of the inner core density field. However, any net rotation results in a gravitational torque between the mantle and the inner core; the gravitational torque is associated with a free oscillation in core-mantle angular momentum (Buffett et al., 2000). This gravitational oscillation represents a rotational perturbation about the planetary rotation axis (figure 5.3 b).

The response of the model to the gravitational torque on the inner core displays resonant amplification at periods corresponding to the natural frequencies in of the system. The resonances are superimposed on the resonance associated with gravitational coupling between the inner core and mantle. The peak response of

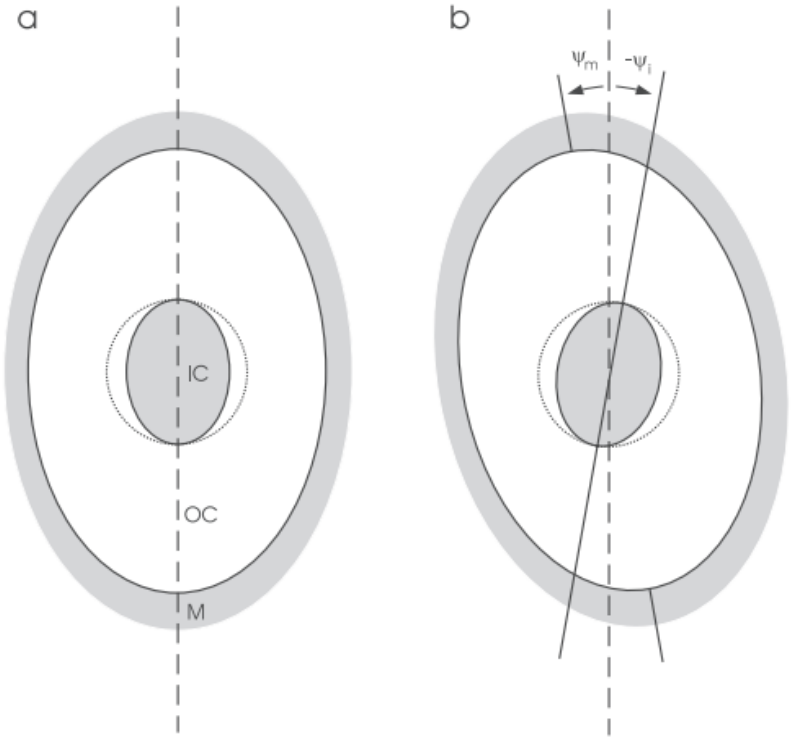

Figure 5.3: Equatorial cross section of the inner core (IC), outer core (OC) and mantle (M) in the equilibrium (a) and perturbed (b) state (Mound and Buffett, 2003).

the system occurs in the vicinity of the natural period of the gravitational mode, called *mode A*, which depends on physical properties of the core and lowermost mantle (Mound et al., 2003). The oscillation identified by Abarca del Rio et al. (2000) of about six-to-seven years is consistent with the expected signal of *mode A* for certain combinations of the core-mantle physical parameters.

Ding et al., 2018, were the first to identify the SYO in global GPS records, by using 38 time series of the Up component and 31 of the Horizontal north and east components (acquired from the Jet Propulsion Laboratory network), over the period 1995-2015. They estimated a 4.3 mm ($\pm$1.7 mm) GPS Up displacement and stated that it exists in GPS surface deformation a manifestation of a westward rotary propagating wave of the sectorial spherical harmonic pattern of degree-2 order-2 (Y_{22}). This was interpreted as a harmonic oscillation in longitude, or the intrinsic rotational mode of axial libration of the inner core relative to the Earth's diurnal spin with a periodicity of about 6 years. In other words, the mantle-inner core gravitational (MICG) coupling causes a rotary westward motion with period of about 6 years in the Earth's outer core and the induced pressure deforms the core-mantle boundary and produces displacements at the Earth's surface that

can be detected by GPS networks (Ding et al., 2018).

Ding (2019), identified eight long period signals by using two datasets, the first one is a yearly LOD time series over the period 1962-2016 and the second one was obtained from the analysis of the Earth Orientation Parameters EOPC04 (`ftp://hpiers.obspm.fr/eop-pc/eop`) dataset. The most relevant for this thesis are the periods of about 6, 8.5 and 18.6 years. A 8.6 years periodic signal was also found by Duan and Huang in 2020. They stated that this EYO presents an unexpected long-term increasing trend and it should be attributed to a possible continuous excitation of unknown nature. Additionally, it was found to closely associate with geomagnetic jerks, which means that the EYO and the geomagnetic jerks may result from a same physical source, i.e. the equatorial quasi-geostrophic Alfvèn waves (Duan et al., 2020).

Regarding the possible relation between the SYO and the EYO and the geomagnetic jerks, R. d. Holme et al. (2005), found that specific jerks were consistent with the sudden changes in the ΔLOD in the 1962–2005 time-span and, in 2013, they confirmed that the sudden changes (jumps) in their SYO time series might have been triggered by geomagnetic jerks. Duan et al. (2020), claimed that they did not identify any possible excited event for the SYO since 1962 and suggested that it was discontinuously excited with a random 50-100 years time interval. They found that the peaks/valleys of the EYO were consistent with some jerks, concluding that the EYO could be used to predict jerks. Ding et al., 2021, by using the 1962–2020 ΔLOD time series from the EOPC04 data set (Bizouard et al., 2019, the atmospheric angular momentum (AAM) data set (Salstein et al., 1993), the oceanic angular momentum dataset (OAM, Gross et al., 2005) and the hydrological angular momentum data set (HAM, based on the Land Surface Discharge Model; Dill, 2008), concluded that, although, the geomagnetic jerks did not have good consistency with the peaks/valleys of the SYO and EYO, they did have some consistency with the sudden changes in the SYO and EYO time series and in their corresponding excitation sequences. This means that the jerks might be possible excitation source for the two oscillations.

5.4 Lunar effects

The Earth suffers deformations due to the gravitational attraction of the celestial bodies and the redistribution of water mass occurring by the action of the

ocean tides (Marotta et al., 2019).

Over interannual time scale, two precessions associated with the orbit of the Moon cause variations of the high tides. These variations arise as a result of the 18.61 year lunar nodal cycle (LNC) and the 8.85 year cycle of the lunar perigee (LPC) (Haigh et al., 2011).

The lunar nodal cycle is determined by the relative movement of the plane in which the Moon orbits the Earth (Pugh, 1996). The period of precessions is 18.61 years.

The cycle of lunar perigee is determined by the Moon's elliptical orbit around the Earth, with its phase described by the positions of least and greatest distance known as perigee and apogee, respectively (Pugh, 1996). The line joining perigee and apogee (the line of apsides) advances in the opposite direction of the lunar regression and completes a full revolution in 8.85 years.

Chapter 6

Results and discussion

In this chapter, the results obtained from the analysis described in Chapter 4 are shown and discussed. GPS observations have enabled significant advantages in the description of the processes influencing the vertical surface deformations.

The aim of this work is to identify and interpret the presence of long-period oscillations in GPS Up time series over the European and Mediterranean area. Identifying vertical surface deformations is important in the light of understanding the dynamic processes governing these oscillations and eventually contributing to the realisation of accurate physical models. Removing known and large signals from the GPS Up time series leads to the possibility of identifying and studying weaker signatures.

The main signals identified in the Up component of the GPS time series are the followings:

- oscillations with periods of 2-to-4 years (see Section 6.1 and 6.2);
- oscillation with period of about six years (see Section 6.3);
- oscillations with period of about eight years (see Section 6.4);
- oscillation with period of about 18.6 years (see Section 6.4).

The periodogram was used to identify the frequency and to determine the amplitude of the vertical displacement induced by these signals. The results of the periodogram are composed by a frequency and an amplitude. It allows to have a representation of which signals are the most relevant inside a time series.

The wavelet spectrum allows to identify the periods and to describe the periodicity of the signals. The wavelet spectrum graphic representation shows the period and the variation of the signal intensity (identified in a first analysis by means of the periodogram) over the investigated time-span.

6.1 El Niño/Southern Oscillation (ENSO)

The wavelet analysis (figure 6.1) identified the presence of a $\sim$ 3 years signal in the first principal component of the GPS Up coordinate, manifesting over the period 2006-2014. Pan et al. (2019), found a similar behavior analysing a GPS network over the Eastern Tibetan Plateau (data acquired from the Crustal Movement Observation Network of China (CMONOC-I and CMONOC-II)) and speculated possible ENSO effects.

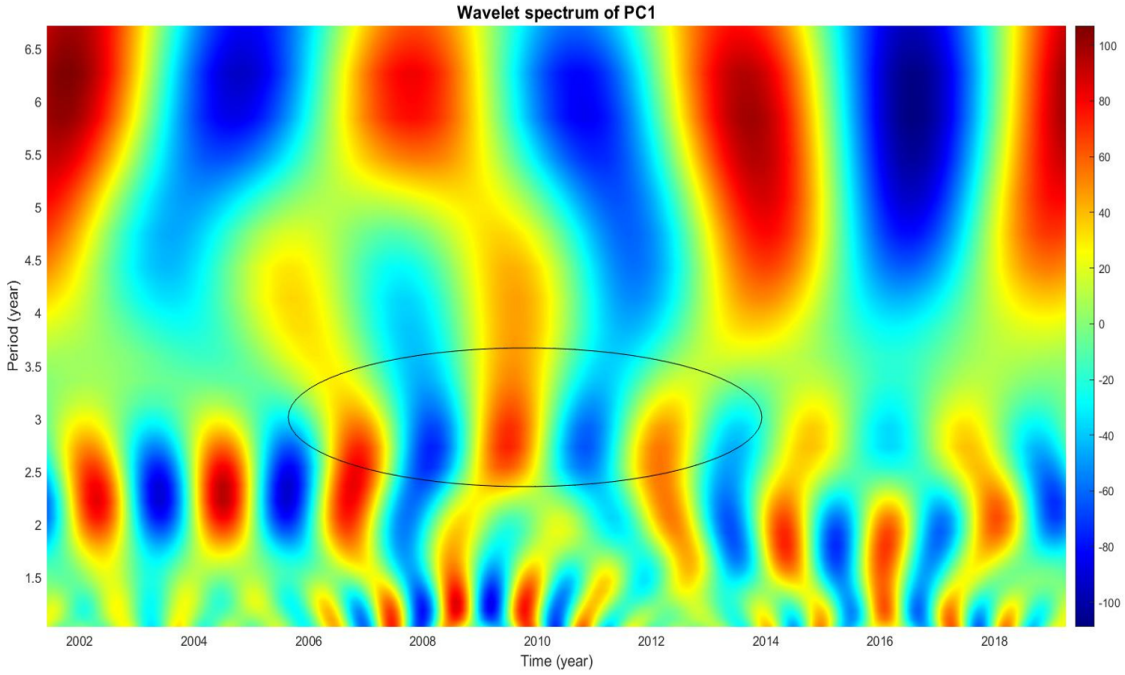

Figure 6.1: Wavelet spectrum of the first principal component of the GPS Up. An oscillation of about 3 years shows up during the period 2006-2014.

ENSO events were detected in the GPS Up time series over the European and Mediterranean area, i.e. Elia et al. (2021). ENSO plays a major role in large-scale variations in precipitation, deforming the Earth's surface through loadings effects.

The Multivariate ENSO Index Version 2 (MEI v2) is a climate index which gives indications of ENSO intensity. The positive and negative phases of ENSO correspond to positive and negative values of the MEI v2 index. In figure 6.2 it is shown the trend of the MEI v2 time series from 1979 to present days (2021).

Few strong La Niña events characterise the MEI v2 time series between 2001 and 2019; the most dominant were active during 1999-2001, 2007-2008 and 2010-

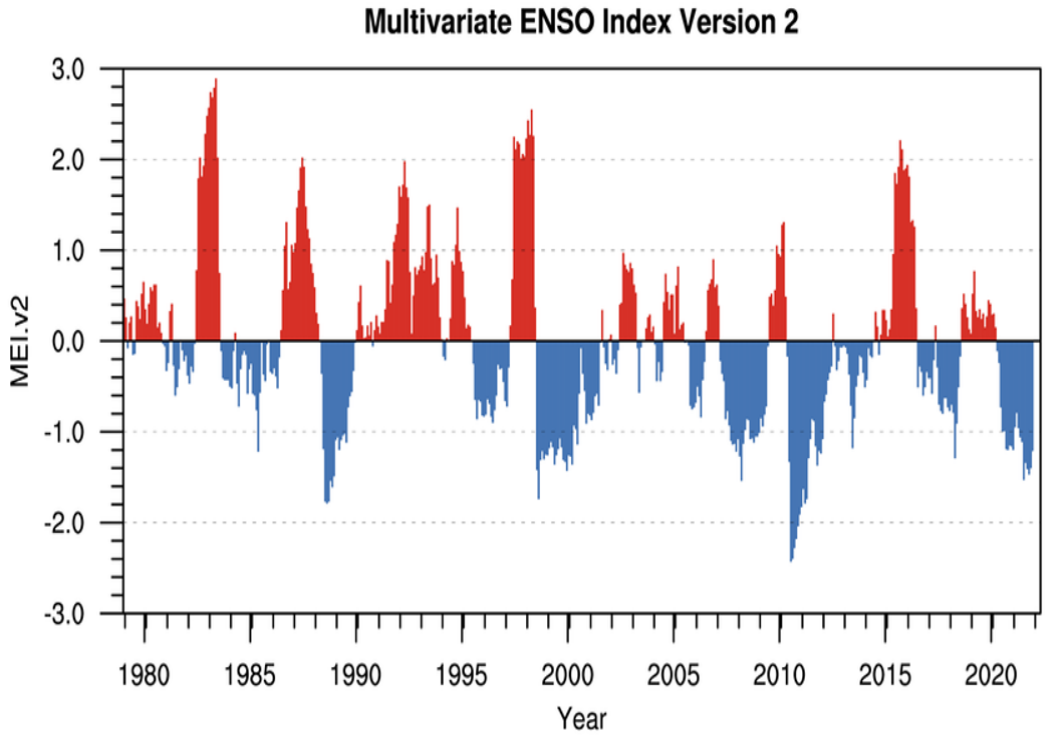

Figure 6.2: MEI v2 time series from 1979 to 2021; red indicates El Niño phase and blue indicates La Niña phase (NOAA PSL).

2011, followed by a moderate event in 2017-2018. One of the most powerful El Niño of the last few years developed at the end of 2014.

Over the European and Mediterranean area, in the period 2010-2018, Elia et al. (2021) found a coherent pattern of anti-correlation between MEI index and the stations height (represented by the first two modes of a monthly PCA analysis) in the area encompassing the Iberian Peninsula, the Mediterranean and central-northern Europe. Instead, the Scandinavian peninsula, Baltic countries and Western Russia pattern shows a positive correlation (figure 6.3). They identified a five years fluctuation in the first time component of the GPS Up coordinate, likely modulated by the sequence of a strong (2010-2011) and a moderate (2017-2018) La Niña, followed by a strong (2014) El Niño.

6.2 Oscillation with period of 2-to-4 years

The results obtained by the frequency analysis conducted in this work (figure 6.4) show a peak in each periodogram of the three principal components (figure 6.4 a, b and c). The frequencies and amplitude value of the signals are shown

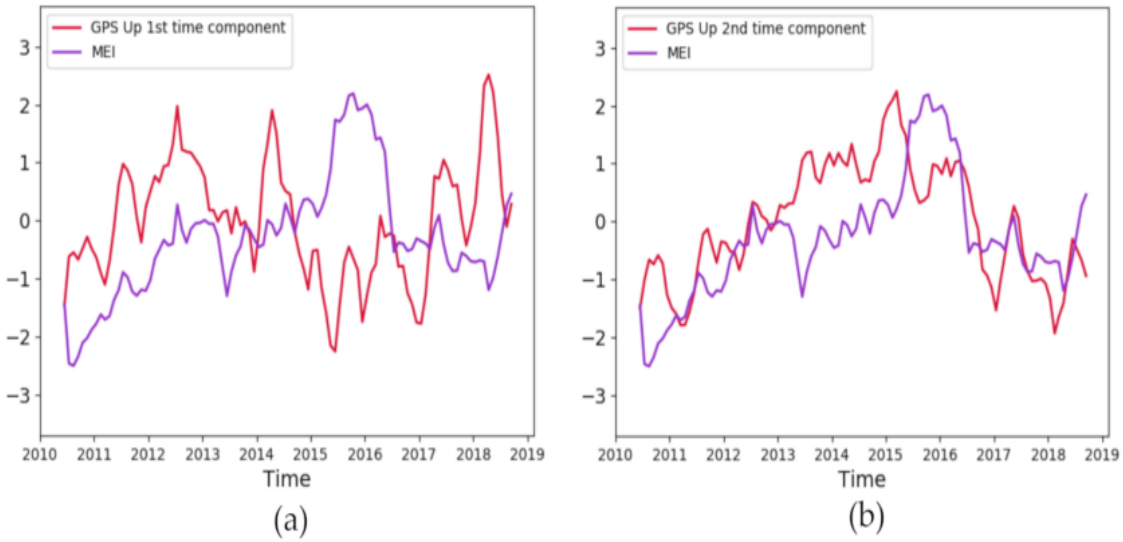

Figure 6.3: Standardized monthly time series of the MEI (purple line) and of the first (a) and second (b) PCA time components of the Up coordinate (from Elia et al., 2021).

in table 6.1. The first principal component identified a stronger signal compared to those of the other components. The wavelet spectra (6.4 d, e and f) show a corresponding signal with a period of 2.49 years with a periodicity of about 2.5 years.

PCs	Frequency (cpy)	Amplitude (mm)
1	0.401	2.777
2	0.445	0.896
3	0.401	0.622

Table 6.1: Frequencies and amplitudes of the QBO signal for each of the first three GPS Up time principal components.

Pan et al. (2015) identified the QBO in the GPS Up component time series by analysing a network of 269 globally distributed GPS stations (acquired from the International GNSS Service (IGS) website and the Chinese continental tectonic environment monitoring network) over the period 2002-2013. They observed that these oscillations were present in 89 GPS stations, mostly located in the Northern Hemisphere (United States of America, Eastern Europe and Southwestern China). By using the Ensemble Empirical Mode Decomposition (EEMD) to the GPS vertical time series to extract the non-linear signals, they estimated, with the autoregressive method, a mean frequency of 0,4315 ($\pm$ 0.018) cpy and a mean vertical displacement of 1,78 ($\pm$ 1) mm.

The results suggest that the source of the identified signal might be the QBO

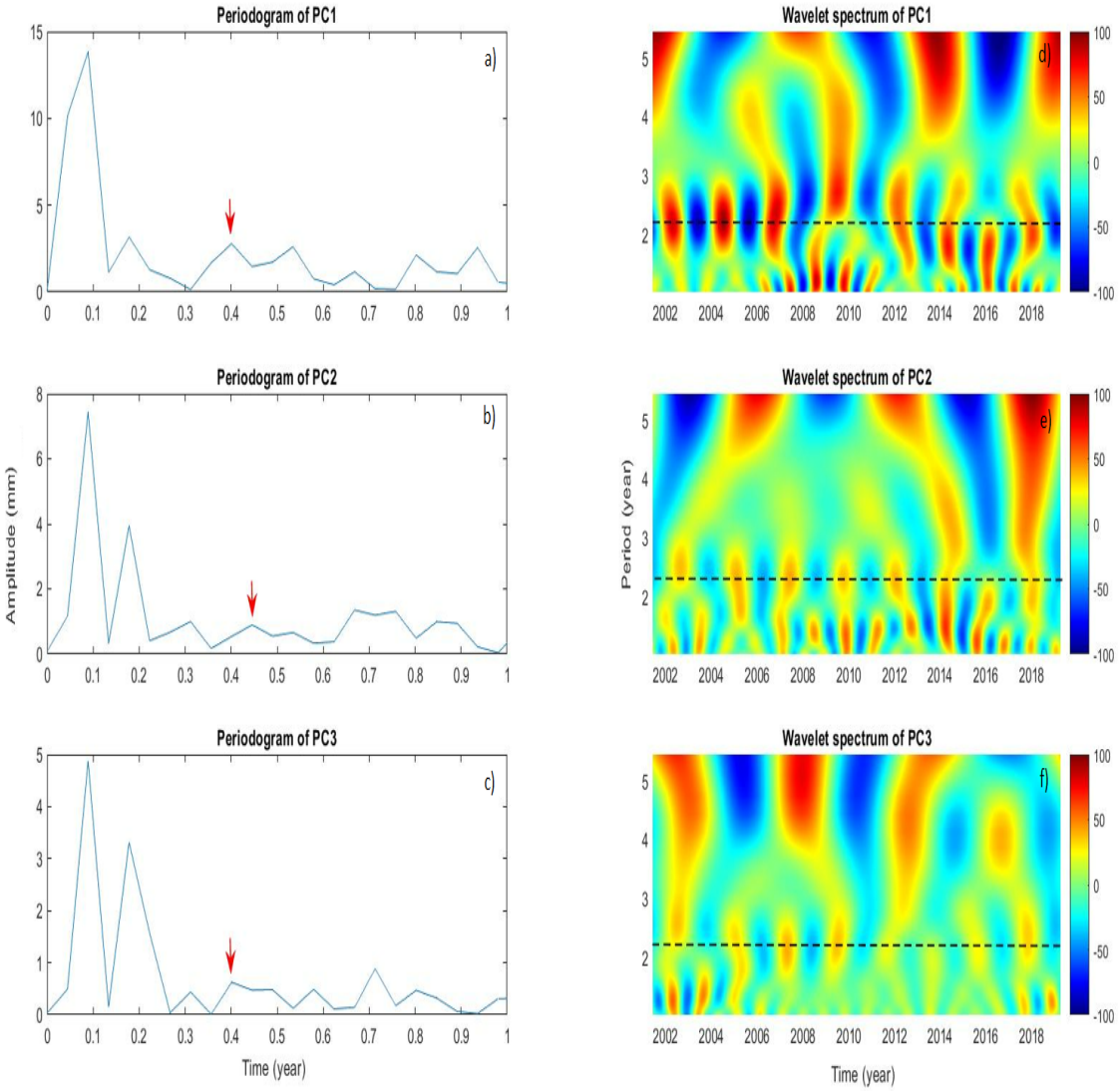

Figure 6.4: Periodograms, on the left side (a, b, c), and the wavelet spectra, on the right side (d, e, f), of the first three principal component of the GPS Up time series. The red arrows in the periodograms indicate the signal in the frequency domain, the dashed black lines in the wavelet spectra show the signal and its variation in the time domain.

since the frequency, the amplitude and the periodicity are in agreement with the results obtained, even if Pan et al. (2015) identified the presence of the QBO only in some of the GPS Up coordinate time series of the stations located in Eastern Europe. The impacts of the QBO on the North Atlantic and Mediterranean area had been confirmed and studied, in relation to storm tracks, by Asbaghi et al. (2017).

To model the non-linear signals and show that the QBO signals indeed exist in the GPS Up coordinate time series, loading models can be used to compute surface deformations. Pan et al. (2015), suggest that the QBO signal is closely related

to atmosphere pressure loading, but the mechanism behind it is still unclear.

6.3 Six year oscillation

The frequency analysis conducted by using the periodogram (see figure 4.1) shows the presence of a peak at 0.1748 cpy in each time series of the first three principal components (table 6.2). This signal is confirmed by the wavelet analysis and it is associated to a period of about six years. More specifically, it is described by a signal of period 5.72 years, with an associated GPS vertical displacement of 3.47 ± 0.41 mm. This value is in agreement, in terms of frequency, amplitude and periodicity, with the results observed by Ding et al. (2018), and Pan et al. (2019), who argued that this signal might be related to the oscillations with period of about six years induced by a rotary westward motion in the Earth's outer core.

PCs	Frequency (cpy)	Amplitude (mm)
1	0.1748	3.161
2	0.1748	3.943
3	0.1748	3.313

Table 6.2: Frequencies and amplitudes of the SYO signal for each of the first three GPS Up time principal components, derived from the periodograms.

The first two PCA time components of the GPS Up time series are shown in figure 6.5 and 6.6. They explain almost 90% of the total variability. The first time component of the GPS Up time series was approximated by the about six years oscillation described by the blue line (figure 6.5 a), which is the least-squares spline approximation with a period of 5.72 years. It was built by applying a least-square approximation with cubic splines to the maxima and minima values of the oscillation phases obtained by the wavelet spectrum. The wavelet analysis allowed to determine the years when this signal has a positive or negative phase and it shows its periodicity. The blue curve shows three maxima (end of 2001, 2008 and 2014) and three minima (2004, 2011 and 2017), corresponding to the red and blue poles in the wavelet analysis (figure 6.5 b), respectively.

Ding et al. (2018) identified a signal with a period of 5.9 years and a vertical surface displacement of amplitude 4.7 ($\pm$ 1.7) mm by analysing a global GPS array (acquired from the Jet Propulsion Laboratory (JPL) website) and a ΔLOD global dataset over the period 1995-2015. They conducted a parallel study on

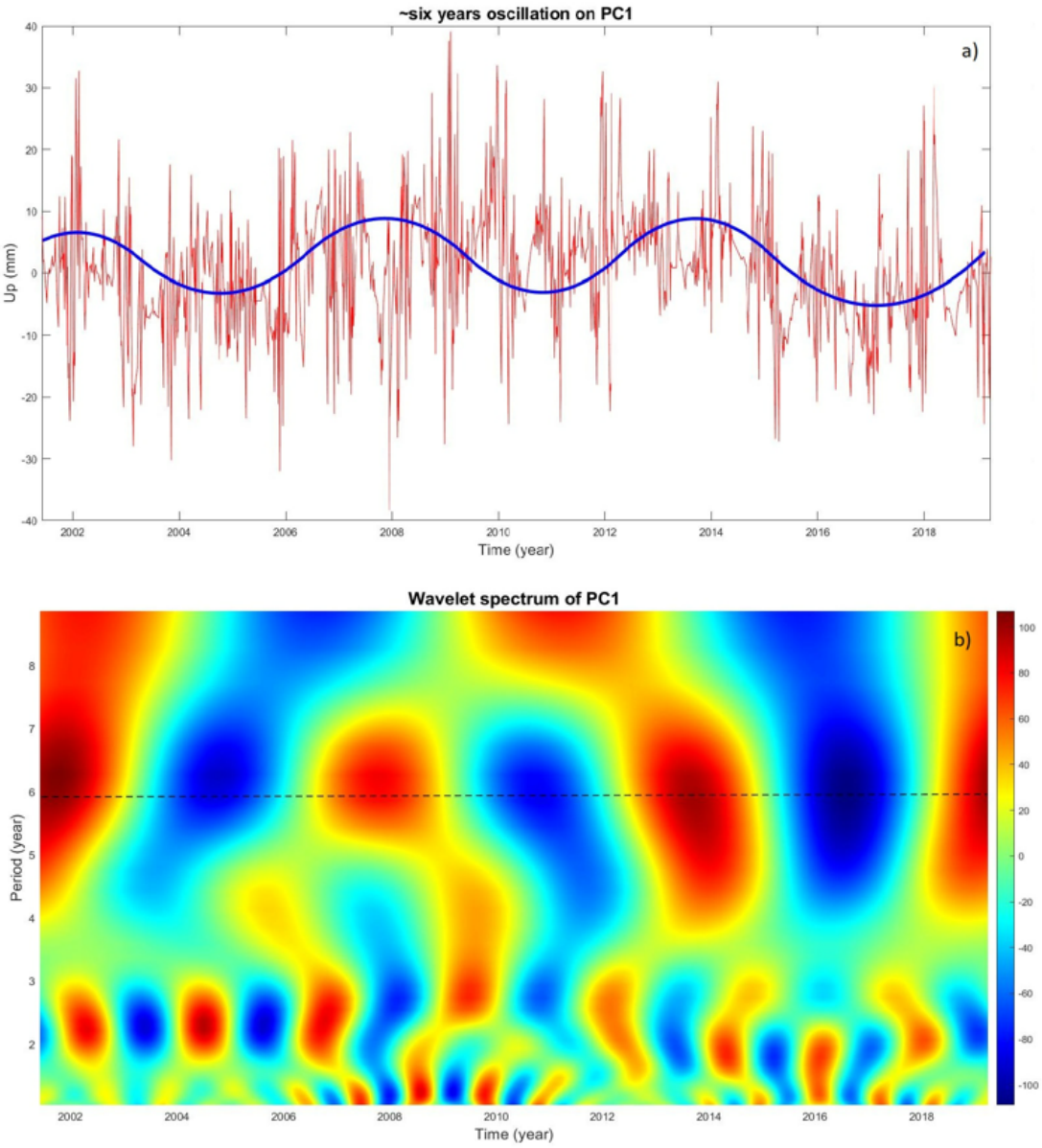

Figure 6.5: a) The 5.7 years signal (blue curve) in the PCA second time component of the GPS Up time series; the blue curve is the least-squares spline approximation with a period of 5.7 years; b) wavelet analysis, the black dashed line identifies an about six years oscillation in the wavelet spectrum.

geomagnetic records (provided by the World Data Centre for Geomagnetism) over the period 1990-2010.5, identifying a signal with a period of 5.9 ($\pm$ 0.07) years. The detected 5.9 years westward rotary motion of the Earth's global interior could be associated to the inner-core oscillation and the SYO found in the ΔLOD.

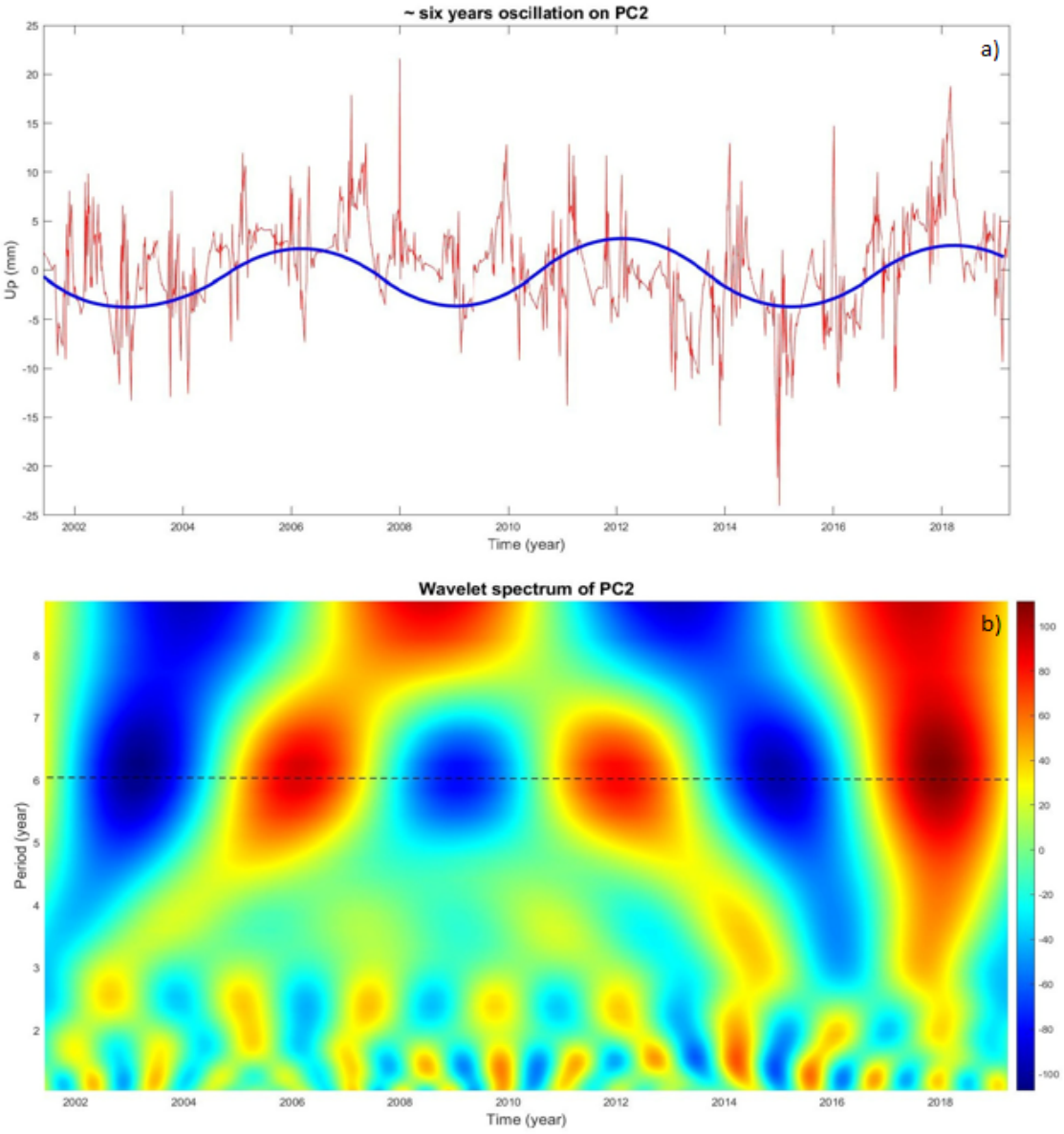

Figure 6.6: a) The 5.7 years signal (blue curve) in the PCA second time component of the GPS Up time series; the blue curve is the least-squares spline approximation with a period of 5.7 years; b) wavelet analysis, the black dashed line identifies an about six years oscillation in the wavelet spectrum.

6.4 Eight and 18.6 year oscillations

The analysis conducted with the real-valued Morlet wavelet shows the presence of a 8-9 years oscillation. This signal has the same phase behavior as the about six years oscillation. In figure 6.7 and 6.8 this signal is shown, respectively for the first and second PCA time components. The signal in the first principal component of the GPS Up coordinate shows two negative phases (2006 and 2016) and two positive phases (2002 and 2011), with a periodicity of about nine years. This signal shows a lower amplitude respect to the about six year oscillation signal identified in the same principal component, which is consistent with the results obtained by Ding (2019) and Hsu et al. (2021), studying the long-period signals in the ΔLOD time series.

An oscillation with a period of about eight years has been identified by analysing ΔLOD dataset (Ding, 2019; Duan et al., 2020; Ding et al., 2021) and it might be explained by the gravitational coupling between the Earth's mantle and the inner core, such as the SYO. The physical process causing this signal is still not clearly demonstrated.

An oscillations with period of 8.85 years has been associated with the effects caused by the interaction between Moon and Earth, particularly by the cycle of the lunar perigee. Moreover, the 18.6 years signal generated by the lunar nodal cycle has been detected in tide gauge observations (Haigh et al., 2011; Peng et al., 2019). Ocean tides produce periodic variations in both the Earth's surface displacement and the gravity field. Additionally, the ocean tides produce a secondary deformational effect due to associated periodic water mass redistribution, known as ocean tide loading, which is observable in surface displacement and gravity (Matviichuk et al., 2020). Therefore GPS is able to detect these type of effects and record them in the time series.

The wavelet analysis managed to identify a 18.6 years signal (figure 6.9). The 18.6 years signal has a positive phase in 2010. The first PCA component of the GPS Up time series shows a maximum around 2010.

The identification of signals with periods of about eight and 18.6 years suggest the presence of effects perturbing the Earth's surface, but they can not yet be explained by means of GPS time series. The available GPS time series data are not yet long enough to study periodic multi-decadal signals such as this case. This might also be the reason why the periodogram can not identify peaks related to

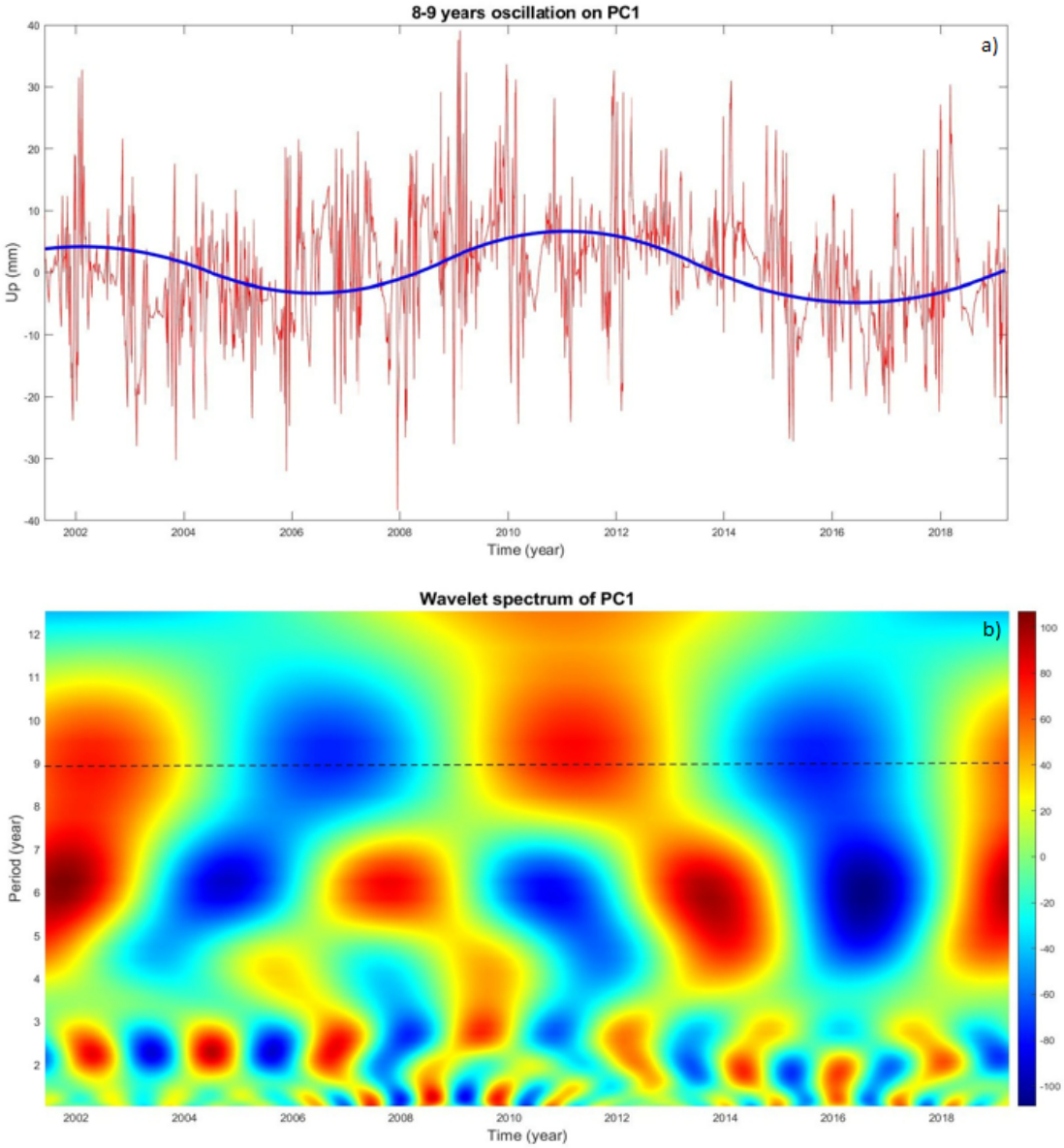

Figure 6.7: a) The 8-9 year oscillation (blue line) in the PCA first time component of the GPS Up time series; the blue curve is the least-squares spline approximation with period of 8-9 years; b) wavelet analysis, the black dashed line identifies an about eight years oscillation in the wavelet spectrum.

this signal.

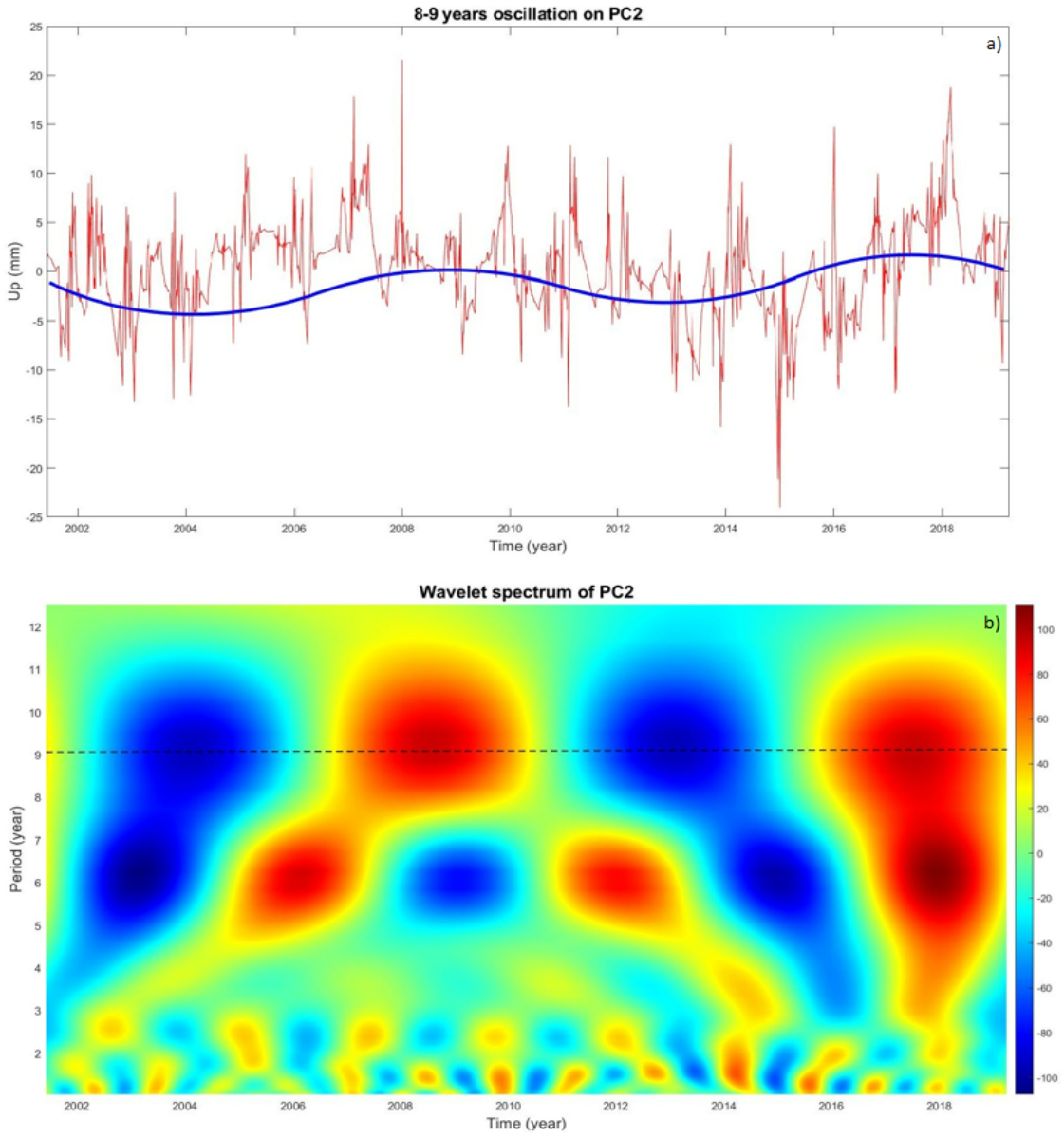

Figure 6.8: a) The 8-9 years oscillation (blue line) in the PCA second time component of the GPS Up time series; the blue curve is the least-squares spline approximation with a period of 8-9 years; b) wavelet analysis, the black dashed line identifies an about eight years oscillation in the wavelet spectrum.

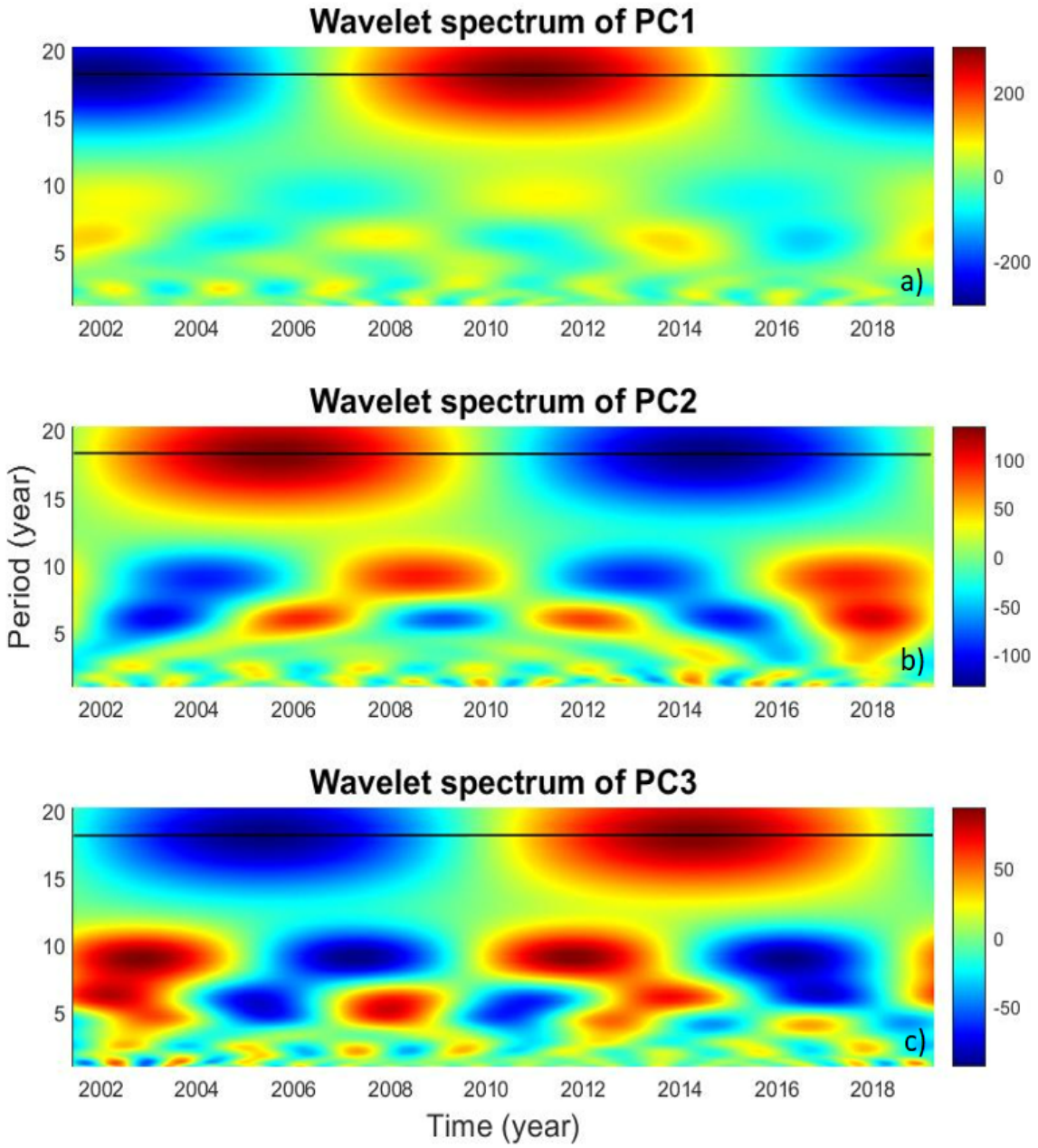

Figure 6.9: The 18.6 years signal (black line) in the wavelet spectrum of the first three principal components of the GPS Up coordinate.

Conclusions

The Earth's surface undergoes deformations due to different geophysical and geological processes. In this thesis, GPS vertical displacements were studied to identify long period signals and understand their possible nature. Thirty-six stations were selected in the European and Mediterranean area, chosen to create a network as homogeneous as possible over a time span of at least eighteen years of data. The data series cover the period from May 30, 2001 to March 27, 2019 so that the time series can be representative of interannual and intradecadal variations.

The coordinate analysed in this study is the height of the GPS stations because it is the one that can more easily explain loading/unloading effects.

The time series underwent a pre-processing phase where the individual linear trend and the mean annual cycle were removed in order to detect interannual and intradecadal variations. The principal component analysis (PCA) was applied to identify the principal modes of space and time variability of the GPS Up coordinate. The first three modes of variability explain about the 90% of the total variability.

Each principal component of the time series of the GPS Up coordinate underwent a frequency analysis carried out both with the periodogram and the real-valued Morlet wavelet transform. The first was used to identify the signal frequency and the amplitude of the of vertical displacement, in order to have a representation of the most relevant signals in the time series. The second one identifies the periods and describes the periodicity of the signals over the investigated time span.

Interannual and intradecadal signals were identified in the GPS Up coordinate time series over the Europe and Mediterranean area. The study allows to identify and likely attribute at least three long-period oscillations over the period 2001-2019.

In the GPS Up time series of the first three principal components, oscillations characterised by a period of about 2.5 years were identified. In addition, the time series of the first principal component shows a signal with period of about

three years over the time interval 2006-2014, which could be related to the ENSO phenomenon as already identified in the European and Mediterranean area by Elia et al. (2021).

The analysis confirmed the presence of a signal with period of about six years (5.72 years), identified in each of the three first principal components. The related vertical displacement turns out to be 3.47 $\pm$ 0.41 mm. This signal might be related to oscillations with period of about six years induced by a rotary westward motion in the Earth's outer core. This would cause a pressure deforming the core-mantle boundary and producing displacements at the Earth's surface that can be identified by means of GPS observations (Ding et al., 2018; Pan et al., 2019).

Longer period signals were also identified by the wavelet transform. Signals with period in the order of 8-9 years and 18.6 years.

The results show of the presence of interannual signals with period of 2-to-4 years, over Europe and Mediterranean area, whose nature needs to be adequately understood. The possible sources might be related to atmospheric and hydrological loading displacements, which are important factors to be monitored in the light of climate change. The about six years oscillation, in Europe and the Mediterranean area, has been identified for the first time in this work and it is consistent with the results published in recent studies for different areas. Concerning longer period oscillations, the study suggests the presence of signals with period in the order of 8-9 years and 18.6 years, identified, until now, with the use of different and longer records (e.i ΔLOD, AAM, tide gauges). These signals need further confirmation because the present length of the GPS time series is still too short when compared to the periods involved.

Bibliography

Abarca del Rio, R, D Gambis, and DA Salstein (2000)
"Interannual signals in length of day and atmospheric angular momentum". In: *Annales Geophysicae*. Vol. 18. 3. Springer-Verlag, pp. 347–364.

Asbaghi, Ghorban, Mohammad Joghataei, and Ali R Mohebalhojeh (2017)
"Impacts of the QBO on the North Atlantic and Mediterranean storm tracks: An energetic perspective". In: *Geophysical Research Letters* 44.2, pp. 1060–1067.

Baarda, W (1968)
"A testing procedure for use in geodetic networks". In: *Pub. on Geod., New Series* 2.5.

Baldwin, Casey M, David A Beauchamp, and Chad P Gubala (2002)
"Seasonal and diel distribution and movement of cutthroat trout from ultrasonic telemetry". In: *Transactions of the American Fisheries Society* 131.1, pp. 143–158.

Baldwin, MP, LJ Gray, TJ Dunkerton, K Hamilton, PH Haynes, WJ Randel, JR Holton, MJ Alexander, I Hirota, T Horinouchi, et al. (2001)
"The quasi-biennial oscillation". In: *Reviews of Geophysics* 39.2, pp. 179–229.

Bartholy, J and R Pongrácz (2006)
"Regional effects of ENSO in central/eastern Europe". In: *Advances in Geosciences* 6, pp. 133–137.

Bertiger, Willy, Yoaz Bar-Sever, Angie Dorsey, Bruce Haines, Nate Harvey, Dan Hemberger, Michael Heflin, Wenwen Lu, Mark Miller, Angelyn W Moore, et al. (2020)
"GipsyX/RTGx, a new tool set for space geodetic operations and research". In: *Advances in space research* 66.3, pp. 469–489.

Bizouard, Christian, Sébastien Lambert, César Gattano, Olivier Becker, and Jean-Yves Richard (2019)
"The IERS EOP 14C04 solution for Earth orientation parameters consistent with ITRF 2014". In: *Journal of Geodesy* 93.5, pp. 621–633.

Björnsson, H and SA Venegas (1997)
"A manual for EOF and SVD analyses of climatic data". In: *CCGCR Report* 97.1, pp. 112–134.

Boehm, Johannes and Harald Schuh (2004)
"Vienna mapping functions in VLBI analyses". In: *Geophysical Research Letters* 31.1.

Bruni, S, Susanna Zerbini, F Raicich, M Errico, and E Santi (2014)
"Detecting discontinuities in GNSS coordinate time series with STARS: case study, the Bologna and Medicina GPS sites". In: *Journal of geodesy* 88.12, pp. 1203–1214.

Buffett, Bruce A and Gary A Glatzmaier (2000)
"Gravitational braking of inner-core rotation in geodynamo simulations". In: *Geophysical Research Letters* 27.19, pp. 3125–3128.

Chao, B Fong (1988)
"Correlation of interannual length-of-day variation with El Niño/Southern Oscillation, 1972–1986". In: *Journal of Geophysical Research: Solid Earth* 93.B7, pp. 7709–7715.

Chao, B Fong (1989)
"Length-of-day variations caused by El Nino-Southern Oscillation and quasi-biennial oscillation". In: *Science* 243.4893, pp. 923–925.

Dam, Tonie van, J Wahr, PCD Milly, AB Shmakin, Geoffrey Blewitt, D Lavallée, and KM Larson (2001)
"Crustal displacements due to continental water loading". In: *Geophysical Research Letters* 28.4, pp. 651–654.

De Boor, Carl and Carl De Boor (1978)
A practical guide to splines. Vol. 27. springer-verlag New York.

Defraigne, P, Véronique Dehant, and John Matthew Wahr (1996)
"Internal loading of an inhomogeneous compressible Earth with phase boundaries". In: *Geophysical Journal International* 125.1, pp. 173–192.

Dill, Robert (2008)
"Hydrological model LSDM for operational Earth rotation and gravity field variations". In.

Ding, Hao (2019)
"Attenuation and excitation of the 6 year oscillation in the length-of-day variation". In: *Earth and Planetary Science Letters* 507, pp. 131–139.

Ding, Hao, Yachong An, and Wenbin Shen (2021)
"New evidence for the fluctuation characteristics of intradecadal periodic signals in length-of-day variation". In: *Journal of Geophysical Research: Solid Earth* 126.2, e2020JB020990.

Ding, Hao and Benjamin F Chao (2018)
"A 6-year westward rotary motion in the Earth: Detection and possible MICG coupling mechanism". In: *Earth and Planetary Science Letters* 495, pp. 50–55.

Donoho, David L (1995)
"De-noising by soft-thresholding". In: *IEEE transactions on information theory* 41.3, pp. 613–627.

Duan, Pengshuo and Chengli Huang (2020)
"On the mantle-inner core gravitational oscillation under the action of the electromagnetic coupling effects". In: *Journal of Geophysical Research: Solid Earth* 125.2, e2019JB018863.

Ebdon, RA and RG Veryard (1961)
"Fluctuations in equatorial stratospheric winds". In: *Nature* 189.4767, pp. 791–793.

Elia, Letizia, Susanna Zerbini, and Fabio Raicich (2021)
"Interannual Variability of GPS Heights and Environmental Parameters over Europe and the Mediterranean Area". In: *Remote Sensing* 13.8, p. 1554.

Forte, Alessandro M, Robert L Woodward, and Adam M Dziewonski (1994)
"Joint inversions of seismic and geodynamic data for models of three—dimensional mantle heterogeneity". In: *Journal of Geophysical Research: Solid Earth* 99.B11, pp. 21857–21877.

Gazeaux, Julien, Simon Williams, Matt King, Machiel Bos, Rolf Dach, Manoj Deo, Angelyn W Moore, Luca Ostini, Elizabeth Petrie, Marco Roggero, et al. (2013)
"Detecting offsets in GPS time series: First results from the detection of offsets in GPS experiment". In: *Journal of Geophysical Research: Solid Earth* 118.5, pp. 2397–2407.

Glatzmaier, Gary A and Paul H Roberts (1996)
"Rotation and magnetism of Earth's inner core". In: *Science* 274.5294, pp. 1887–1891.

Greiner-Mai, Hans (1993)
"Decade variations of the Earth's rotation and geomagnetic core-mantle cou-

pling". In: *Journal of geomagnetism and geoelectricity* 45.11-12, pp. 1333–1345.

Gross, Richard S, Ichiro Fukumori, and Dimitris Menemenlis (2005)
"Atmospheric and oceanic excitation of decadal-scale Earth orientation variations". In: *Journal of Geophysical Research: Solid Earth* 110.B9.

Haigh, Ivan D, Matt Eliot, and Charitha Pattiaratchi (2011)
"Global influences of the 18.61 year nodal cycle and 8.85 year cycle of lunar perigee on high tidal levels". In: *Journal of Geophysical Research: Oceans* 116.C6.

Hawkins, Douglas M (1980)
Identification of outliers. Vol. 11. Springer.

Heck, B (1981)
"Der Einfluß einzelner Beobachtungen auf das Ergebnis einer Ausgleichung und die Suche nach Ausreißern in den Beobachtungen". In: *Avn* 88.1, pp. 17–34.

Hide, Raymond and Jean O Dickey (1991)
"Earth's variable rotation". In: *Science* 253.5020, pp. 629–637.

Hinderer, J, H Legros, D Jault, and J-L Le Mouël (1990)
"Core-mantle topographic torque: a spherical harmonic approach and implications for the excitation of the Earth's rotation by core motions". In: *Physics of the earth and planetary interiors* 59.4, pp. 329–341.

Holme, R de and O De Viron (2005)
"Geomagnetic jerks and a high-resolution length-of-day profile for core studies". In: *Geophysical Journal International* 160.2, pp. 435–439.

Holme, Richard (1998)
"Electromagnetic core—mantle coupling—I. Explaining decadal changes in the length of day". In: *Geophysical Journal International* 132.1, pp. 167–180.

Hsu, Can-Can, Peng-Shuo Duan, Xue-Qing Xu, Yong-Hong Zhou, and Cheng-Li Huang (2021)
"On the ~ 7 year periodic signal in length of day from a frequency domain stepwise regression method". In: *Journal of Geodesy* 95.5, pp. 1–15.

Ineson, SySCAIFE and AA Scaife (2009)
"The role of the stratosphere in the European climate response to El Niño". In: *Nature Geoscience* 2.1, pp. 32–36.

Jolliffe, Ian T and Jorge Cadima (2016)
"Principal component analysis: a review and recent developments". In: *Philo-*

sophical Transactions of the Royal Society A: Mathematical, Physical and Engineering Sciences 374.2065, p. 20150202.

Kumar, Praveen and Efi Foufoula-Georgiou (1997)

"Wavelet analysis for geophysical applications". In: *Reviews of geophysics* 35.4, pp. 385–412.

Lehmann, Rüdiger (2013)

"3 σ-rule for outlier detection from the viewpoint of geodetic adjustment". In: *Journal of Surveying Engineering* 139.4, pp. 157–165.

Liao, DC and H Greiner-Mai (1999)

"A new ΔLOD series in monthly intervals (1892.0–1997.0) and its comparison with other geophysical results". In: *Journal of geodesy* 73.9, pp. 466–477.

Lin, Jialin and Taotao Qian (2019)

"A new picture of the global impacts of El Nino-Southern oscillation". In: *Scientific reports* 9.1, pp. 1–7.

Marotta, Giuliano Sant'Anna, Mário Alexandre de Abreu, Ana Cristina Oliveira Cancoro de Matos, João Francisco Galera Monico, and George Sand Leão Araújo de França (2019)

"Analysis of Ocean Tide Loading Estimated from the GPS Coordinate Time Series: A Case Study for the Belém, Brasılia, Eusébio, Manaus and Santa Maria Stations, Brazil". In: *Brazilian Journal of Geophysics* 37.4, pp. 565–578.

Matviichuk, Bogdan, Matt King, and Christopher Watson (2020)

"Estimating ocean tide loading displacements with GPS and GLONASS". In: *Solid earth* 11.5, pp. 1849–1863.

McKinley, Sky and Megan Levine (1998)

"Cubic spline interpolation". In: *College of the Redwoods* 45.1, pp. 1049–1060.

Mishra, Sidharth Prasad, Uttam Sarkar, Subhash Taraphder, Sanjay Datta, D Swain, Reshma Saikhom, Sasmita Panda, and Menalsh Laishram (2017)

"Multivariate statistical data analysis-principal component analysis (PCA)". In: *International Journal of Livestock Research* 7.5, pp. 60–78.

Mound, J.E. and B.A. Buffett (2003)

"Interannual oscillations in length of day: Implications for the structure of the mantle and core". In: *Journal of Geophysical Research: Solid Earth* 108.B7.

Mound, J.E. and B.A. Buffett (2006)

"Detection of a gravitational oscillation in length-of-day". In: *Earth and Planetary Science Letters* 243.3-4, pp. 383–389.

Ordonez, Celestino, J Martınez, JR Rodrıguez-Pérez, and Andria Reyes (2011)
"Detection of outliers in GPS measurements by using functional-data analysis". In: *Journal of Surveying Engineering* 137.4, pp. 150–155.

Pan, Yuanjin, Ruizhi Chen, Hao Ding, Xinyu Xu, Gang Zheng, Wenbin Shen, YiXin Xiao, and Shuya Li (2019)
"Common mode component and its potential effect on GPS-inferred three-dimensional crustal deformations in the eastern Tibetan plateau". In: *Remote Sensing* 11.17, p. 1975.

Pan, Yuanjin, Wen-Bin Shen, Hao Ding, Cheinway Hwang, Jin Li, and Tengxu Zhang (2015)
"The quasi-biennial vertical oscillations at global GPS stations: Identification by ensemble empirical mode decomposition". In: *Sensors* 15.10, pp. 26096–26114.

Pan, Yuanjin, Wen-Bin Shen, Cheinway Hwang, Chaoming Liao, Tengxu Zhang, and Guoqing Zhang (2016)
"Seasonal mass changes and crustal vertical deformations constrained by GPS and GRACE in Northeastern Tibet". In: *Sensors* 16.8, p. 1211.

Peng, Dongju, Emma M Hill, Aron J Meltzner, and Adam D Switzer (2019)
"Tide gauge records show that the 18.61-year nodal tidal cycle can change high water levels by up to 30 cm". In: *Journal of Geophysical Research: Oceans* 124.1, pp. 736–749.

Pope, Allen J (1976)
The statistics of residuals and the detection of outliers. US Department of Commerce, National Oceanic and Atmospheric Administration ...

Pugh, D.T. (1996)
Tides, surges and mean sea-level (reprinted with corrections). John Wiley & Sons, Ltd. URL: `https://eprints.soton.ac.uk/19157/`.

Reed, Thomas B (1961)
"Induction-coupled plasma torch". In: *Journal of Applied Physics* 32.5, pp. 821–824.

Rioul, Olivier and Martin Vetterli (1991)
"Wavelets and signal processing". In: *IEEE signal processing magazine* 8.4, pp. 14–38.

Rodionov, Sergei N (2004)
"A sequential algorithm for testing climate regime shifts". In: *Geophysical Research Letters* 31.9.

Russell, Brian and Jiajun Han (2016)

"Jean Morlet and the continuous wavelet transform". In: *Morlet and the Continuous Wavelet Transform CREWES Research Report* 28.1946, pp. 1–15.

Salstein, David A, Deirdre M Kann, Alvin J Miller, and Richard D Rosen (1993)

"The sub-bureau for atmospheric angular momentum of the International Earth Rotation Service: A meteorological data center with geodetic applications". In: *Bulletin of the American Meteorological Society* 74.1, pp. 67–80.

Seeber, Günter (2008)

Satellite geodesy. de Gruyter.

Shaman, Jeffrey and Eli Tziperman (2011)

"An atmospheric teleconnection linking ENSO and southwestern European precipitation". In: *Journal of Climate* 24.1, pp. 124–139.

Soycan, M. and T. Ocalan (2011)

"A REGRESSION STUDY ON RELATIVE GPS ACCURACY FOR DIFFERENT VARIABLES". In: *Survey Review* 43.320, pp. 137–149. DOI: 10.1179/003962611X12894696204867. URL: https://doi.org/10.1179/003962611X12894696204867.

Stix, M and PH Roberts (1984)

"Time-dependent electromagnetic core-mantle coupling". In: *Physics of the earth and planetary interiors* 36.1, pp. 49–60.

Tang, W, X-H Xue, J Lei, and X-K Dou (2014)

"Ionospheric quasi-biennial oscillation in global TEC observations". In: *Journal of Atmospheric and Solar-Terrestrial Physics* 107, pp. 36–41.

Tary, Jean Baptiste, Roberto Henry Herrera, and Mirko van der Baan (2018)

"Analysis of time-varying signals using continuous wavelet and synchrosqueezed transforms". In: *Philosophical Transactions of the Royal Society A: Mathematical, Physical and Engineering Sciences* 376.2126, p. 20170254.

Teixell, Antonio, Giovanni Bertotti, Dominique Frizon de Lamotte, and Mohamed Charroud (2009)

"The geology of vertical movements of the lithosphere: An overview". In: *Tectonophysics* 475.1, pp. 1–8.

Tiwari, VM, N Srinivas, and B Singh (2014)

"Hydrological changes and vertical crustal deformation in south India: Inference from GRACE, GPS and absolute gravity data". In: *Physics of the Earth and Planetary Interiors* 231, pp. 74–80.

vanDam, Tonie M., Geoffrey Blewitt, and Michael B. Heflin (1994)
"Atmospheric pressure loading effects on Global Positioning System coordinate determinations". In: *Journal of Geophysical Research: Solid Earth* 99.B12, pp. 23939–23950. DOI: https://doi.org/10.1029/94JB02122. eprint: https://agupubs.onlinelibrary.wiley.com/doi/pdf/10.1029/94JB02122. URL: https://agupubs.onlinelibrary.wiley.com/doi/abs/10.1029/94JB02122.

Wang, Linsong, Chao Chen, Jinsong Du, and Tongqing Wang (2017)
"Detecting seasonal and long-term vertical displacement in the North China Plain using GRACE and GPS". In: *Hydrology and Earth System Sciences* 21.6, pp. 2905–2922.

Zou, Rong, Qi Wang, Jeffrey T Freymueller, Markku Poutanen, Xuelian Cao, Caihong Zhang, Shaomin Yang, and Ping He (2015)
"Seasonal hydrological loading in southern Tibet detected by joint analysis of GPS and GRACE". In: *Sensors* 15.12, pp. 30525–30538.

Acknowledgements

Al termine di questo elaborato, desidero esprimere un sentito ringraziamento alla Professoressa Susanna Zerbini, alla Professoressa Damiana Lazzaro e alla Dottoressa Letizia Elia per avermi costantemente seguito e supportato nel lavoro di ricerca, aiutandomi con la loro esperienza e con preziosi consigli.
Ringrazio, inoltre, la mia famiglia, i miei amici e tutte le persone che a modo loro hanno condiviso con me questo percorso.

Appendices

Appendix A

GPS Stations list

GPS station name	Latitude (°)	Longitude (°)
ALME	36.8525	-2.4594
BOR1	52.2770	17.0735
CANT	43.4720	-3.7981
CASC	38.6934	-9.4185
ELBA	42.7529	10.2111
EUSK	50.6741	6.7635
GAIA	41.1060	-8.5891
GLSV	50.3642	30.4967
HERS	50.8673	0.3363
HOFN	64.2673	-15.1979
INGR	41.8281	12.5148
LAMA	53.8924	20.6699
LEIJ	51.3540	12.3741
LLIV	42.4781	1.9731
MALL	39.5526	2.6246
MAN2	48.0186	0.1553
MAR6	60.5951	17.2585
MARS	43.2788	5.3538
METS	60.2175	24.3953
MSEL	44.5200	11.6465
PENC	47.7896	19.2815
POLV	49.6026	34.5429
PTBB	52.2962	10.4597
REYK	64.1388	-21.9555
SMID	55.6406	9.5593

SOFI	42.5561	23.3947
SONS	39.6754	-3.9640
SPT0	57.7150	12.8913
STAS	59.0177	5.5986
TORI	45.0634	7.6613
TRDS	63.3714	10.3192
VARS	70.3364	31.0312
VIL0	64.6978	16.5599
VIS0	57.6539	18.3673
WSRT	52.9146	6.6045
ZIMM	46.8771	7.4653

Table A.1: GPS station name, latitude and longitude.